FINAL REPORT

Surface Modified TiO2 Obscurants for Increased Safety and Performance

SERDP Project WP-2150

NOVEMBER 2012

Dr. Steven Oldenburg
Mr. John Holecek
nanoComposix, Inc.

SERDP
DOD ▪ EPA ▪ DOE

REPORT DOCUMENTATION PAGE

Form Approved
OMB No. 0704-0188

1. REPORT DATE *(DD-MM-YYYY)*	2. REPORT TYPE	3. DATES COVERED *(From - To)*
30-11-2012	Final Report	20-06-2012 – 30/11/2012

4. TITLE AND SUBTITLE
Surface Modified TiO2 Obscurants for Increased Safety and Performance

5a. CONTRACT NUMBER
W912HQ-11-P-0037

5b. GRANT NUMBER

5c. PROGRAM ELEMENT NUMBER

6. AUTHOR(S)
Dr. Steven Oldenburg
Mr. John Holecek

5d. PROJECT NUMBER
WP-2150

5e. TASK NUMBER

5f. WORK UNIT NUMBER

7. PERFORMING ORGANIZATION NAME(S) AND ADDRESS(ES)

nanoComposix, Inc
4878 Ronson CT STE K
San Diego, CA 92111

8. PERFORMING ORGANIZATION REPORT NUMBER

9. SPONSORING / MONITORING AGENCY NAME(S) AND ADDRESS(ES)
Strategic Environmental Research and Development Program
4800 Mark Center Drive, Suite 17D08
Alexandria, VA 22350-3605

10. SPONSOR/MONITOR'S ACRONYM(S)
SERDP

11. SPONSOR/MONITOR'S REPORT NUMBER(S)

12. DISTRIBUTION / AVAILABILITY STATEMENT
Approved for public release; distribution is unlimited

13. SUPPLEMENTARY NOTES

14. ABSTRACT

Numerical modeling predicts that titanium dioxide (TiO_2) based obscurants could produce MECs that exceed 10 m^2/g across the visible portion of the spectrum and gFOMs of 25 m^2/cm^3 if TiO_2 particles with a narrow size distribution were fabricated and dispersed in a non-agglomerated format. The overall goal of this project was to develop a visible obscurant using low toxicity TiO_2 particles that improves upon the performance of existing powder based visible obscurant grenades by a factor of 5. This goal was achieved by chemically and physically improving the dry powder fill material in a TiO_2 grenade and investigating new methods of disseminating TiO_2 nanoparticles to reduce agglomeration when aerosolized.

Several methods to synthesize TiO_2 were developed and evaluated, one yielded discrete 184 nm diameter particles with an 18% CV. A variety of commercially available TiO_2 powders were also acquired, processed, and functionalized with surface chemistries designed to minimize surface adhesion and to optimize dissemination. A wide variety of surface modified TiO_2 powders were packed at precisely controlled pressures into various container geometries. The best performing material was Tiona RCL-9 TiO_2 (Cristal Global) coated in solution with cyclic azasilanes, lyophilized to remove the solvent without agglomerating the nanomaterials, compressing into a thin puck using a ram with 500 psi pressure, and pneumatically disseminating with a burst of 1000 psi air. Using this optimized approach, gFOMs of up to 4 m^2/cm^3 were obtained, compared to 0.6 m^2/cm^3 for the currently fielded M106 grenade (a factor of 6 improvement). Continued improvement in deagglomerating commercial powders followed by surface functionalization and effective dissemination has the potential to increase performance closer to the theoretical gFOM for TiO_2 based smokes which is 25.9 m^2/cm^3. If successful, such improvements would allow for the generation of a rapid, safe, and effective new class of obscuration devices that would exceed HC based obscurant devices in performance.

15. SUBJECT TERMS
Obscurant, visible, IR, smoke, TiO2, aerosol, particle, surface modification, coatings, extinction

16. SECURITY CLASSIFICATION OF:			17. LIMITATION OF ABSTRACT	18. NUMBER OF PAGES	19a. NAME OF RESPONSIBLE PERSON
a. REPORT	b. ABSTRACT	c. THIS PAGE			Dr. Steven Oldenburg
					19b. TELEPHONE NUMBER *(include area code)* 619-890-0704

Table of Contents

LIST OF FIGURES

Figure **Page**

LIST OF TABLES

Table **Page**

LIST OF ACRONYMS

APS	Aerodynamic Particle Sizer
APTES	aminopropyltrimethoxysilane
CV	Coefficient of Variation (standard deviation / mean)
DCM	Dichloromethane
DI	Deionized
DMDMS	dimethyldimethoxysilane
DPDMS	diphenyldimethoxysilane
ECBC	Edgewood Chemical Biological Center
FZD	Freeze Dry
gFOM	grenade Figure of Merit (m^2/cm^3)
HC	Hexachloroethane
HMDS	hexamethyldimethoxysilane
IR	Infrared wavelength
LabRAM	Lab scale Resonant Acoustic Mixer from Resodyn Corporation
LPM	Liters Per Minute
M106	Currently fielded (Army) visible obscurant grenade
MAG	Multipurpose Aerosol Grenade
MEC	Mass Extinction Coefficient (m^2/g)
NCX	NanoComposix, Inc.
NOTMS	n-octyltrimethoxysilane
NPT	National Pipe Thread
OD	Outer Diameter
ODTMS	Octadecyl trimethoxysilane
PDD	Pneumatic Dissemination Device
PFOTMS	Perfluorooctyltrimethoxysilane
PFPTMS	Pentafluorophenyltrimethoxy silane
PTFE	Polytetrafluoroethylene
RCL-9	Titanium Dioxide material from Cristal Global
RH	Relative Humidity
RPM	Revolutions Per Minute

SEED	SERDP Exploratory Development
SERDP	Strategic Environmental Research and Development Program
SIB1932.4	N-n-BUTYL-AZA-2,2-DIMETHOXYSILACYCLOPENTANE
SMPS	Scanning Mobility Particle Sizer
SRI	Standford Research Institute
TEM	Transmission Electron Microscope
TPG	2,4,6-trinitrophloroglucinol
UV-Vis	Ultraviolet-visible wavelengths

KEYWORDS

Obscurant, visible, IR, smoke, TiO2, aerosol, particle, surface modification, coatings, extinction

ACKNOWLEDGEMENTS

The financial support of the Department of Defense Strategic Environmental Research and Development Program is hereby acknowledged.

1 Abstract

Military smokes that efficiently obscure light across visible wavelengths and have low environmental impact and human health toxicity have not yet been developed. Hexachloroethane (HC) smokes have excellent obscuration performance with mass extinction coefficients (MECs) of > 3 m^2/g across visible wavelengths, but are toxic and have limited use. A non-toxic obscuration grenade, the M106, has been produced by the Army and is currently used for visible obscurant applications. The MEC of M106 devices tested in a 190 m^3 chamber at the Edgewood Chemical Biological Center (ECBC) averages 1.7 m^2/g in the 400 – 700 nm regime with a grenade figure of merit (gFOM; a measure of fielded performance) of 0.67 m^2/cm^3. Numerical modeling predicts that titanium dioxide (TiO_2) based obscurants could produce MECs that exceed 10 m^2/g across the visible portion of the spectrum and gFOMs of 25 m^2/cm^3 if TiO_2 particles with a narrow size distribution were fabricated and dispersed in a non-agglomerated format.

The overall goal of this SERDP SEED project was to develop a visible obscurant using low toxicity TiO_2 particles that improves upon the performance of existing powder based visible obscurant grenades by a factor of 5. This goal was achieved by chemically and physically improving the dry powder fill material in a TiO_2 grenade and investigating new methods of disseminating TiO_2 nanoparticle to reduce agglomeration when aerosolized.

Several methods to synthesize TiO_2 were developed and evaluated. One method produced stable monodisperse particles with mean diameters of 20 nm and 20% coefficient of variation (CV) and another method yielded discrete 184 nm diameter particles with an 18% CV. A variety of commercially available TiO_2 powders were also acquired, processed, and functionalized with surface chemistries designed to minimize surface adhesion and to optimize dissemination. Uncoated TiO_2 particles are hydrophilic, and after coating with long chain silane groups can be rendered hydrophobic which improves their dispersibility. Techniques for coating TiO_2 particles both in solution and as a dry powder were successfully developed.

A wide variety of surface modified TiO_2 powders were packed at precisely controlled pressures into various container geometries. The packed powders were disseminated into a custom built 2.5 m^3 aerosol chamber using various dispersal methods that are optimized to generate high shear forces and minimize the agglomeration of the aerosolized materials. The high improvement due to surface functionalization was Tiona RCL-9 TiO_2 (Cristal Global) coated in solution with cyclic azasilanes, lyophilized to remove the solvent without agglomerating the nanomaterials, compressing into a thin puck using a ram with 500 psi pressure, and pneumatically disseminating with a burst of 1000 psi air. Using this optimized approach, gFOMs of up to 4 m^2/cm^3 were obtained, compared to 0.6 m^2/cm^3 for the currently fielded M106 grenade (a factor of 6 improvement). It is important to note that these gains in performance were obtained using surface coatings on commercially developed powders that were still agglomerated, and continued improvement in deagglomerating commercial powders followed by surface functionalization and effective dissemination has the potential to increase performance closer to the theoretical gFOM for TiO_2 based smokes which is 25 m^2/cm^3. If successful, such improvements would allow for the generation of a rapid, safe, and effective new class of obscuration devices that would exceed HC based obscurant devices in performance.

2 Objective

The currently fielded visible obscurant device, the M106 grenade (**Figure 2.1**), uses a powdered TiO_2 obscurant that is loose filled, vibrationally organized, and pyrotechnically disseminated using a center burster configuration. This device has relatively low yields (23.0 ± 9.0%) and poor dissemination resulting in a low gFOM (0.63 m^2/cm^3). NanoComposix has developed a three pronged approach to address the shortcomings of the currently fielded device and improve the gFOM using a cost effective and scalable approach: 1) commercial TiO_2 powders are surface functionalized to reduce the surface energy and improve yields; 2) surface modified materials are dried, processed, and compressed into the dissemination device to maximize the fill fraction; 3) obscurant material is dispersed using a optimized geometry and high shear pneumatic burst dissemination method. Results from this integrated approach show a gFOM of 4.0 m^2/cm^3, a 6-fold improvement over the M106.

Figure 2.1: Cutaway view of M106 grenade showing center burster with surrounding obscurant fill.

3 Background

3.1 Pyrotechnic Smoke Performance

Pyrotechnic smokes are effective screens in the visible (400 – 700 nm) and near-IR (700 – 1100 nm) portion of the spectrum. HC is a pyrotechnic mixture of hexachloroethane (C_2Cl_6), zinc oxide (ZnO), and aluminum (Al) [NRC1997]. In typical formulations, approximately equal parts of C_2Cl_6 and ZnO zinc oxide are mixed with 6 - 9% by weight aluminum powder. When heated, a propagation reaction between the aluminum and C_2Cl_6 generates $AlCl_3$. The $AlCl_3$ reacts with ZnO to form a hot $ZnCl_2$ gas. When the gas cools below the condensation temperature of $ZnCl_2$, particulates are formed that rapidly absorb water from the surrounding medium. The resulting aerosol of droplets has a particle size distribution that is ideal for attenuating the visible portion of the spectrum [Hartman 1995].

The extinction coefficient of HC smokes at various humidities is shown in **Figure 3.1**. The MEC peaks at ~50% relative humidity (RH) with a value of 3.66 m^2/g. The yield factor, a measure of mass of material aerosolized divided by the mass of material launched, increases from 1.39 at 5% RH to 10.49 at 95% RH. Yield factors above 1 are unique to condensing smokes where the liquid that is extracted from the atmosphere increases the mass of the generated aerosol. The drop-off in extinction at high RH is due to the drop size being greater than the optimal size (0.3 - 0.5 μm) for efficiently scattering visible light.

3.2 HC Toxicity

The primary material responsible for toxicity of HC based smokes is the reaction product $ZnCl_2$ formed by an intermediate reaction of $AlCl_3$ with ZnO. Chlorinated vapors including organochlorines also comprise approximately 10.8% of the final mass fraction [DeVaull 1989] and contribute to the toxicity. Inhalation of the astringent and corrosive $ZnCl_2$ vapor inflames the upper respiratory tract [ATSDR 1997, 2005]. The only known cases of fatalities from HC smoke exposures are in confined spaces [Hill 1978]. Pulmonary symptoms include chest constriction, pain, hoarseness with secondary symptoms including elevated pulse, fever, and edema [Donohue 1992]. Acute toxicity may also be associated with the production of $ZnCl_2$ and hydrochloric acid vapors, which can cause lung inflammation, mucosal membrane irritation, dry skin and eyes with smoke exposures >1 hr [Katz 1980, Selden 1994] with hepatotoxicity also reported [Loh 2006]. Repeated exposures to $ZnCl_2$ have been associated with edema, alveolitis, macrophate infiltration, and fibrosis [Brown 1990]. Alveolar carcinoma in mice was predicted at 0.086 mg $ZnCl_2$/kg bw/d. While fatalities are rare, HC smoke exposure has caused death due to acute respiratory distress syndrome and edema of the lungs [Cullumbine 1957]. The toxicity of HC is sufficiently high that the Army is actively searching for safe replacements.

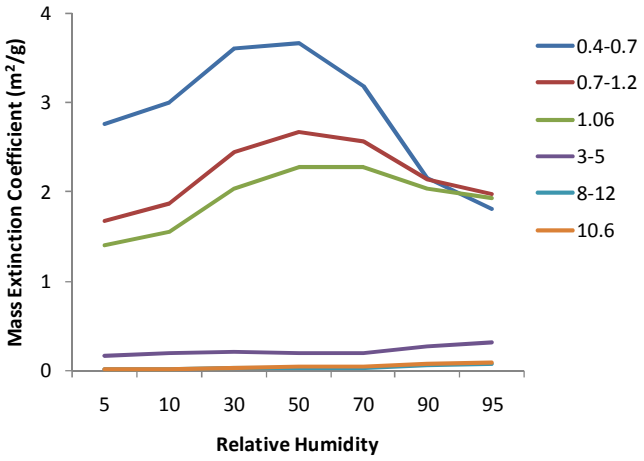

Figure 3.1: Mass extinction coefficient as a function of relative humidity at different wavelength regimes (measured in μm) [NRC 1997].

3.3 Particle Based Obscurants

Particle based obscurants aerosolize solid particulates to generate screening clouds. Various types of particulates are utilized in obscurant munitions including TiO_2 particles in the M106 visible screening grenade and brass flakes in the M76 IR screening grenade. An advantage of particulate based obscurants is that there is flexibility in the size, shape, and material composition of particles that can be aerosolized. Theoretical calculations predict that much higher MECs are obtainable for particle based obscurants than is currently being achieved.

The performance of an obscurant depends not only on the extinction coefficient of the fill, but also on the density at which the material can be packed and how well the material can be disseminated. The Edgewood Obscurant Team uses a figure of merit that is directly related to the predicted field performance of the obscurant grenade. The grenade figure of merit is given by,

$$gFOM = \alpha \rho FY \qquad (1)$$

where α is the extinction per unit mass (MEC) of the obscurant material in m^2/g, ρ is the density of the obscurant material in g/m^3, F is the fill fraction of the obscurant when packed into a grenade, and Y is the percentage of material that is aerosolized after a dissemination event (yield). The units

of the gFOM are m^2/cm^3 which relates to the extinction cross section that can be generated from a cubic centimeter of packed powder.

The M106 is a non-fragmentary visible obscurant grenade that uses Tronox CR-470 TiO_2 nanoparticles packed around an explosive center burster core. The MEC of a M106 grenade averages ~1.7 m^2/g in the visible portion of the spectrum (**Figure 3.2**). The bulk density of TiO_2 is 4 g/cm^3 and the tap density of TiO_2 is 1.2 g/cm^3. A fill fraction of 31% is calculated by dividing the bulk density by the tap density. Measured yields from a functioned device at ECBC are ~31% at ~5 minutes demonstrating that a significant percentage of the launched mass settles during the first tens of seconds after the grenade detonation. The calculated gFOM for the M106 is 0.63 m^2/cm^3.

The results of previous TiO_2 aerosolization studies at nanoComposix using three different dispersion mechanisms are shown in **Figure 3.3**. The venturi Stanford Research Institute (SRI) nozzle is clearly superior to the other launch mechanisms due to the microturbulence at the nozzle exit that deagglomerates the powder. *This data highlights that very large increases in performance can be obtained by simply improving the dissemination characteristics of the powder.*

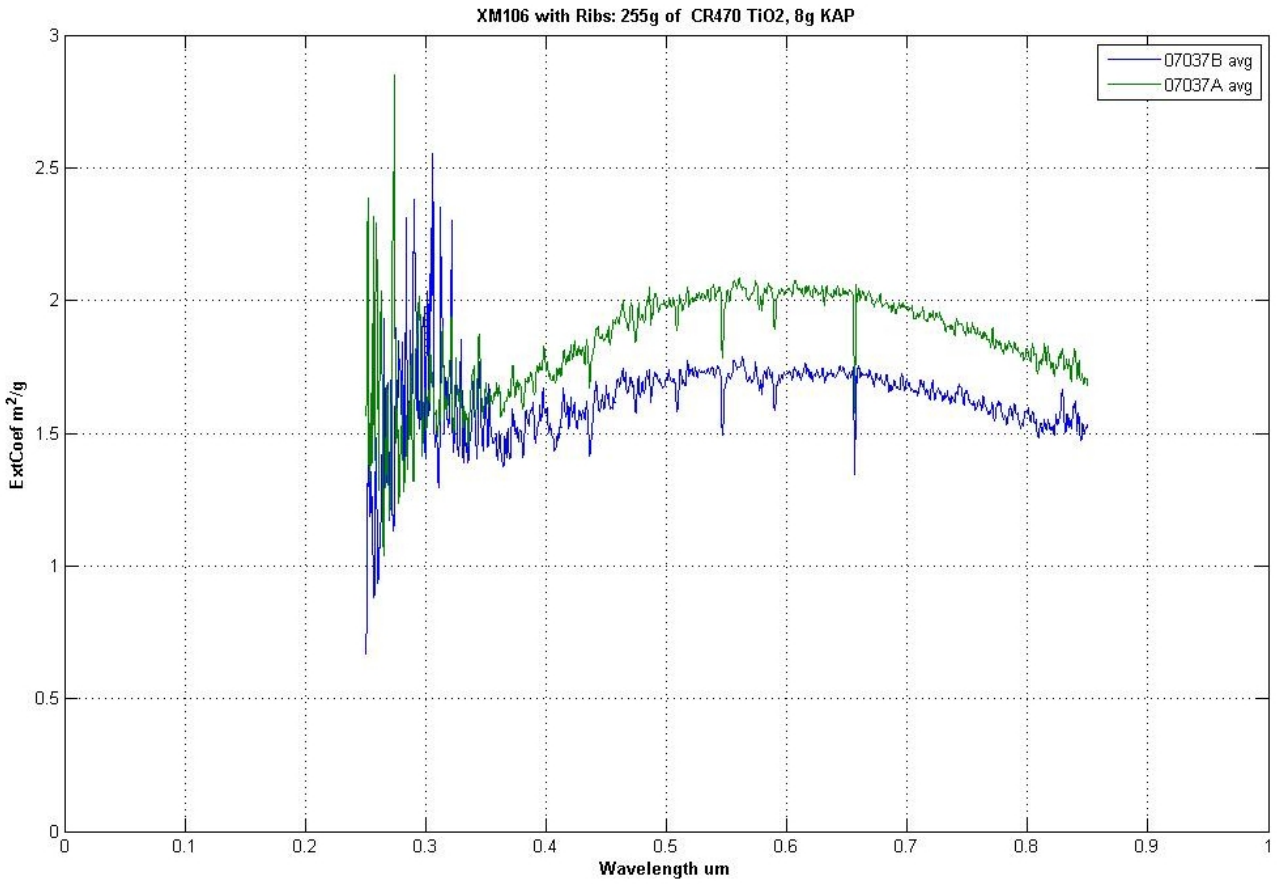

Figure 3.2: Mass extinction coefficient of TiO_2 that remains airborne 5 minutes after M106 dissemination measured at ECBC's 190 m^3 chamber.

When the MEC data shown in **Figure 3.3** is converted to gFOM based on the packed powder density, the gFOM of the TiO_2 launched using the SRI, burst disc, and pneumatic are 4.0 m^2/cm^3, 1.4 m^2/cm^3, and 0.68 m^2/cm^3, respectively. SRI launched TiO_2 has a gFOM >6X that of the M106. This result demonstrates that if dissemination can be improved, a very large obscuration performance increase will be obtained for particle based obscurants. It should be noted that the dissemination conditions under which the high (4.0 m^2/cm^3) value was obtained utilized a venturi nozzle disseminating material at a low mass flow rate (~2 gram per minute into a high flow air stream). While this mass flow rate and dissemination method are not practical for a fielded device, the technique illustrates the magnitude of the performance increase if dissemination issues can be solved.

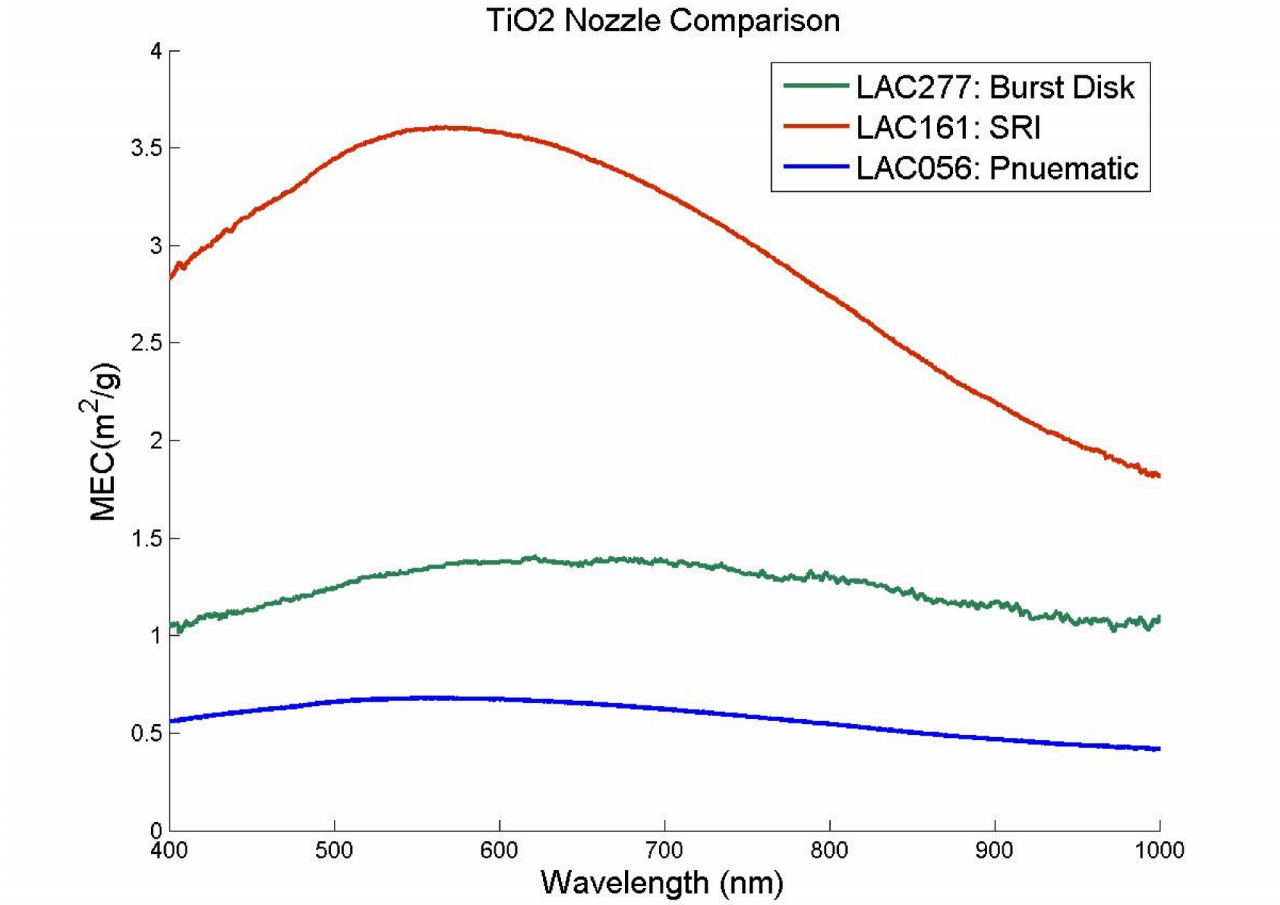

Figure 3.3: Tiona 188 TiO_2 launched using 1000 psi burst disc, 80 psi SRI venturi pump, and 750 psi pneumatic burst via an electronically actuated solenoid valve. MEC values assume 100% of TiO_2 launched remains airborne.

HC smokes have an average MEC of ~3 m^2/g. Liquid fill fractions are equal to 1 and the density of HC is calculated to be 3.5 m^2/g based on 45% HC (ρ = 2.09 g/cm^3), 45% ZnO (ρ = 5.06 g/cm^3) and 10% Al (ρ = 2.7 g/cm^3). gFOM is calculated to be 10.5 m^2/cm^3. It is useful to calculate the theoretical limit of TiO_2 based obscurants to determine if it is possible for particle based smokes to equal or exceed HC performance. Using Mie Scattering theory, the MEC of TiO_2 nanoparticles as a function of particle size was calculated (**Figure 3.4**). Optimal size is ~200 nm and the average extinction across the visible portion of the spectrum at this diameter is 10.1 m^2/g. The maximum fill fraction for spherical particles is 64% which corresponds to an optimal packed powder density of 2.6 g/cm^3. The maximum theoretical gFOM for TiO_2 based smokes is 25.9 m^2/cm^3 which exceeds that of a HC smoke. Numerical modeling of TiO_2 nanoparticle agglomerates using Discrete Dipole algorithms calculates that the MEC rapidly degrades when the particles are agglomerated. When 200 nm particles are clustered into 60 or 330 nanoparticle clusters, the MECs are reduced by 65% and 90%, respectively. This effect is the primary reason for the discrepancy between the theoretical maximum gFOM and measured gFOM of the M106 device, and demonstrates that very large performance increases can be obtained by reducing powder agglomeration.

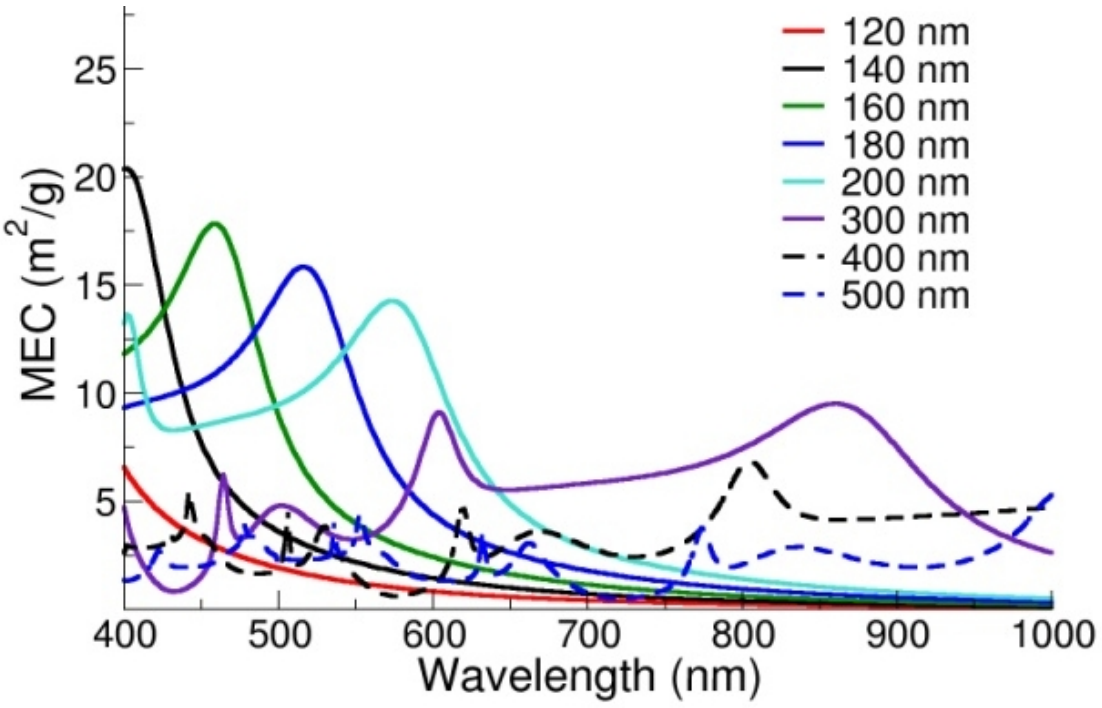

Figure 3.4: Mie theory of individual spheres of TiO_2 (n = 2.74) showing peak MEC values > 14 m^2/g in the visible

4 Materials and Methods

4.1 Custom synthesis and functionalization

TiO_2 is typically prepared by the reaction of $TiCl_4$ with pure oxygen, or isolation from ilmenite by digestion out of the iron component with sulfuric acid. Pure TiO_2 exists in several different crystal morphologies, with the rutile being the most thermodynamically stable and having the highest refractive index. Preparation of titania nanoparticles is achieved by plasma reaction of $TiCl_4$ with oxygen under the appropriate conditions, mechanical attrition of larger particles or by the solution condensation of various titania precursors followed by a thermal annealing to generating the correct crystal phase. The RCL-9 titania is widely available, inexpensive and has high extinction characteristics. Aerosolized obscurant performance may be enhanced through the use of lower surface energy surface groups which reduces aggregation and increases yield during launch. Solution chemistry is an effective way of changing the surface functionality of nanoparticles, and can be applied to nanoparticles that are not agglomerated in solution. The goal of this project is to develop a coating that does not increase the agglomeration of TiO_2 in solution and to dry the suspended nanoparticles using a method that results in a readily aerosolizable powder. Alternatively, dry powders may be surface modified using heated vapors. This approach is attractive from a cost standpoint because it reduces the processing steps required, as the drying is no longer needed.

4.2 Titania synthesis

4.2.1 Discrete unagglomerated anatase seed particles

There were several methods attempted for the synthesis of TiO_2 nanoparticles. The most successful synthesis was the hydrolysis of titanium alkoxide ($Ti(iPrO)_4$) in the presence of tetramethylammonium hydroxide. This synthesis yielded anatase titania nanocrystals. Briefly, 1.14 mmol of $Ti(iPrO)_4$ in 10 mL of anhydrous isopropanol was slowly added via syringe under N_2 to 1.36 mmol of NMe_4OH in 150 mL of milli-Q water at 2 ^oC. This solution was then refluxed at ~160^o C for 6 hours. An aliquot of this solution was centrifuged to remove large particles and in the supernatant was found to be very small titania nanoparticles on the order of ~7 nm with a 20% CV (**Figure 4.1**). Adding multiple aliquots of Ti(iPrO)4 solution over 24 hrs yielded 7 nm, 9.5 nm, and 12.2 nm titania nanoparticles (**Figure 4.2**). When using the 9.5 nm TiO_2 nanoparticles as a seed, particles with diameters of approximately 20 nm with a 20% CV were formed (**Figure 4.3**).

4.2.2 Discrete unagglomerated 200 nm particles

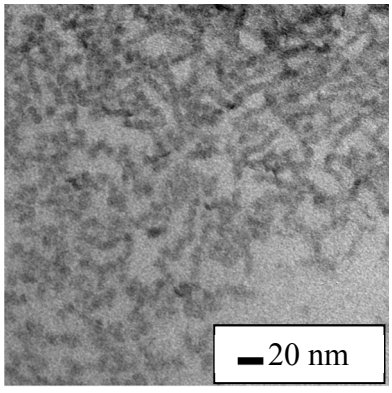

Figure 4.1: 7 nm diameter titania nanoparticles.

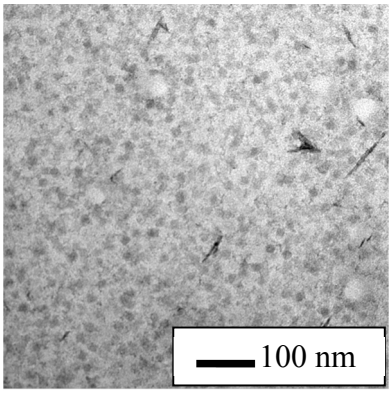

Figure 4.2: 12.2 nm diameter titania nanoparticles.

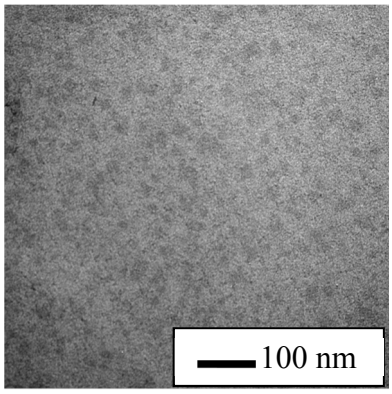

Figure 4.3: 20 nm diameter titania nanoparticles.

Another TiO_2 fabrication method that was investigated was the hydrolysis of titanium tetraethoxide (TEOT) in aqueous ethanol solutions. The size was controlled by the addition of electrolytes. A solution of TEOT in ~50mL of 200 proof ethanol is rapidly combined with a solution of the electrolyte (.05M HCl). The mixture is swirled and placed in a 30 °C water bath during the development of the particles. Using this method, particles with diameters of ~300 nm with a 13% CV were formed. This solution was gently centrifuged ~5 times to remove the remaining reagents before being added to water (**Figure 4.4**). However, when placed in an autoclave, the particles were not stable and were dissociated into smaller TiO_2 particles. A second method used a salt addition to achieve the desired size. 50 mL of 200 proof ethanol was placed in a flask under nitrogen and to this was added 0.1M CsCl salt. This solution was degassed by freeze thaw, brought back up to room temperature and then the TEOT was added to achieve a final concentration of 0.075M. This method yielded particles on the order of 184 nm with an 18% CV (**Figure 4.5**). When processed using centrifugation, the particles dissociated **Figure 4.6**. Based on the TEM images, it appears that the larger particles consist of a number of smaller particles that dissociate with time.

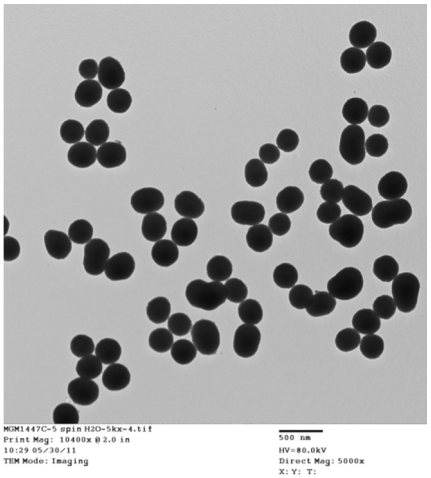

Figure 4.4: 300 nm diameter titania nanoparticles as synthesized.

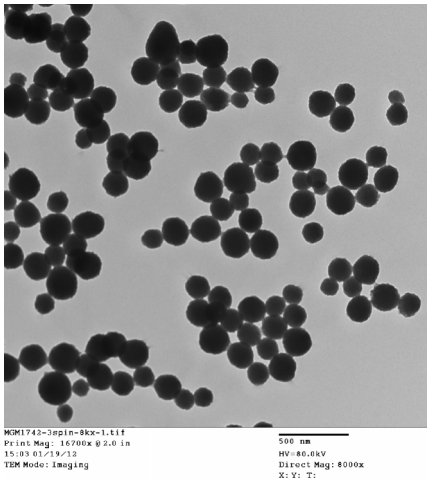

Figure 4.5: Titania nanoparticles after 3 spins.

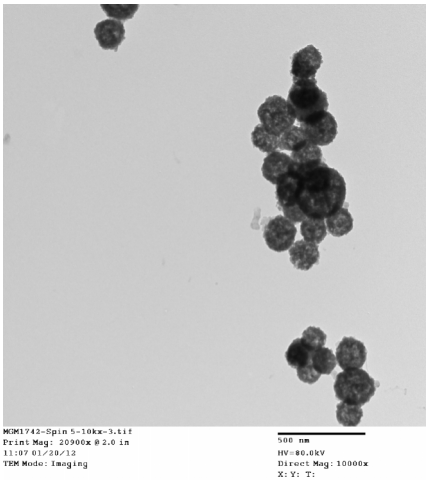

Figure 4.6: Titania nanoparticles after 5 spins.

As our efforts to synthesize titania particles were not successful in producing robust particles of the desired 140 – 300 nm diameter range, subsequent efforts focused on coating commercially synthesized TiO_2.

4.3 Surface functionalization of commercial TiO_2 powders

Agglomeration significantly degrades the performance of aerosolized obscurants. The goal of this project is to coat dried TiO_2 powders with a surface coating that will optimize its extinction properties for both the visible and near IR wavelength spectrum. The imparted surface coating will modify the surface energy and affect the aerosolized agglomeration state. Solution or vapor phase deposition of various silanes and other surface modifiers is utilized to coat the surface of the TiO_2 particles. In order to coat dried powder formulations of TiO_2, the particles must be suspended during the coating process and different means of agitating the TiO_2 during coating were investigated. Powder coating performance was measured by measuring the surface droplet contact angle, which provides a measure of the hydrophobicity of the surface. Additionally, the coated powder was compressed to 500 psi and launched into the nanoComposix chamber using a high pressure solenoid valve. The level of agglomeration state was determined by measuring the yields, MEC, and gFOM.

A wide variety of obscurants have been tested at nanoComposix to understand how their physical and chemical characteristics determine their obscurant performance. TiO_2 based obscurants are an important class of materials due to their high index of refraction, UV performance, and low toxicity. Tiona RCL-9 TiO_2 from Cristal Global was the primary material used in this study due to its high purity and lack of organic coating (**Figure 4.7**).

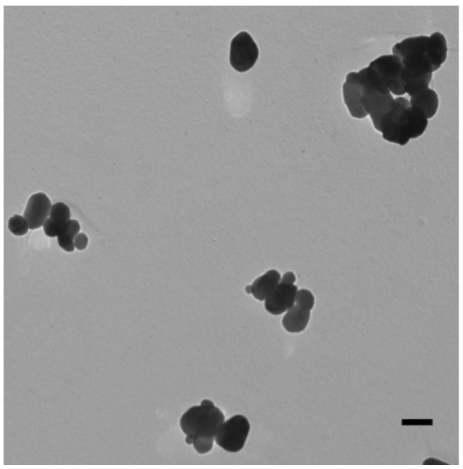

Figure 4.7: TEM image of Tiona RCL-9. Scale bar is 200 nm, and mean particle size is 182 nm.

4.3.1 Surface functionalization of RCL-9 TiO_2 in solution

TiO_2 is an obscurant with strong absorption in the UV region of the spectrum and a high refractive index. The material is cheaply available from a range of vendors in appropriate sizes but is not optimized for aerosol launch. Preliminary experiments suggest that the use of different surface coatings, hydrophobic coatings in particular, may improve the performance of the TiO_2 particles as a smoke with higher yields being observed [DeLacy 2011]. Here we develop methods to surface functionalize TiO_2 particles and measure the performance enhancement of different surface functionalization.

Various surface chemistries designed to lower the surface energy and stiction forces that contribute to agglomeration and reduce the overall per unit mass extinction potential of an obscurant device have been formulated. Generally these surface formulations prevent aggregation by modifying the surface with irregularly shaped functionalization chains that reduce the surface to surface contact potential, hindering the processes that lead to aggregation.

These surface chemistries can generally be grouped into two classes, hydrophobic and hydrophilic, depending on their affinity for absorbing water. RCL-9 as it is manufactured is hydrophilic, in that it wicks water from the air. This is a problem for many reasons. First, moist

TiO_2 is sticky and doesn't readily aerosolize through a venturi pump nozzle, coating all available surfaces with a thick film rather than contributing to aerosol cloud.

With these considerations, DeLacy explored a range of polyol and silane groups to study their effects on obscuration performance [DeLacy 2011]. One specific surface functionalization, Diphenyldimethoxysilane or DPDMS, was found to increase the performance of RCL-9 by around 200% in the visible over uncoated RCL-9 (**Figure 4.8**).

Overall, the surface modifications with hydrophobic alkoxyl silanes performed much better compared the hydrophilic silanes, hence we initially selected to focus our efforts on this class of materials. During the course of our project, we identified the cyclic azasilanes as being ideal candidates for depositing monolayer thickness coatings on nanoparticles [Arkles 2004, Zhu 2012].

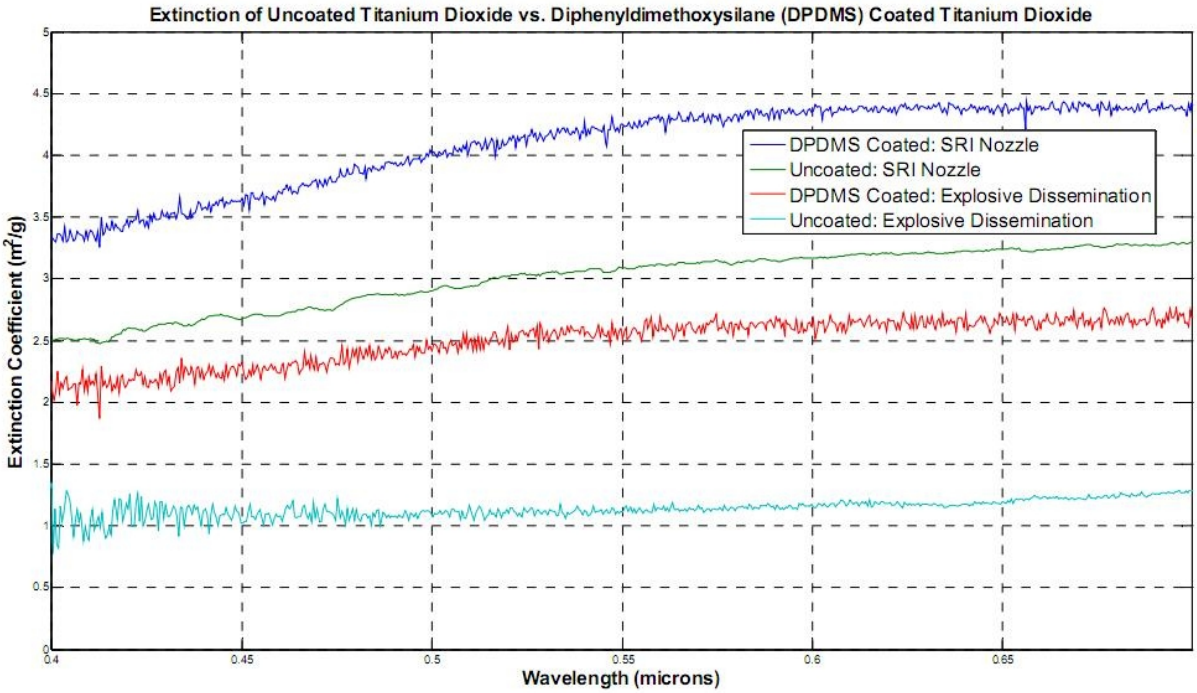

Figure 4.8: Mass extinction coefficients for SRI venturi nozzle and explosively disseminated material, showing a 2x improvement for DPDMS coated RCL-9 over the uncoated material [DeLacy 2011].

4.3.1.1 Cyclic azasilanes

A small batch (~5g) of RCL-9 was functionalized with cyclic azasilanes to produce a hydrophobic coating on the surface and dry the material for in-house chamber measurements. The results from ECBC and Brendan DeLacy show that applying a hydrophobic coating to TiO_2 improves the MEC values relative to uncoated material. Many efforts have been made to coat RCL-9 with alkoxy silanes by solution and vapor deposition with variable and inconsistent results. The recent qualitative observations from mixing cyclic azasilanes with RCL-9 in solution have shown that the reaction proceeds rapidly at room temperature, yielding particles that are readily dispersed in cyclohexane.

Materials:

- 5.041g of TiO_2 RCL-9
- ~150mL of cyclohexane

- ~1.5 g of SIB1932.4
- 750mL Pyrex pan with thermocouple & custom lid

Procedure:

1. Silanize a 250mL round bottom using trichloromethylsilane and DCM.
2. Weigh out 5g of RCL-9 and place in flask when silanization is complete.
3. Pipette ~150mL of cyclohexane into the flask and add a stir bar. Bath sonicate the mixture for about a minute to suspend particles as best as possible. Particle will not be stable in cyclohexane until silane is added.
4. Pipette the azasilane from Schlenk flask (~1.5g) and spike into stirring flask.
5. Sonicate the mixture immediately for roughly 30 seconds to suspend any particles that have fallen out of solution.
6. Place mixture in water bath set to 30^{o}C and RPM=750. Allow reaction to proceed for 30 minutes.
7. Remove flask from bath and transfer contents to a 750mL plastic centrifuge bottle. Use neat cyclohexane and sonication to remove any residual particles in round bottom flask.
8. Centrifuge the mixture at 3800 RPM for 40 minutes. Decant off supernatant and replace with ~150mL of cyclohexane. Sonicate vigorously until there are no visible chunks at the bottom of the bottle.
9. Repeat step #8 for a total of 3 spins.
10. Transfer the final mixture after sonication to a pre-cleaned freeze dryer pan. Place the thermocouple in the mixture and clip with binder clips. Cover the pan with the custom lid that uses perforated aluminum foil and a paper towel to block particles during sublimation.
11. Place the entire pan on the freeze dryer shelf pre-set to -10^{o}C. Allow it to freeze overnight and log the temperature changes.
12. Start the 2 stage compressor after the temperature stability has been verified. Allow to sublimate overnight.
13. Check on the temperature stability the following morning to see if the dry powder is ready to be removed from the freeze dryer.
14. Bring temperature back to 30^{o}C and allow shelves to establish equilibrium for ~1hr. Turn off compressors and allow vacuum to break.
15. Remove the material and quickly transfer to a product bottle for a mass balance. Three grams of the powder will be packed and launched for MEC analysis.

Results: The RCL-9 appeared very hydrophobic based on qualitative observations made during the reaction. Particles were miscible with cyclohexane within minutes of adding the cyclic azasilane. The batch was transferred to centrifuge bottles and spun 3 times to remove any residual azasilane or unreactive species. The final spin was reconstituted with 150 mL of neat cyclohexane and transferred to a freeze drier pan equipped with a thermocouple.

The pan was left to freeze overnight with a thermocouple logging in real time. Temperature was verified the following morning to insure the mixture was completely frozen before pulling vacuum. The vacuum was left to sublimate cyclohexane for at least 24 hours prior to removing the pan.

After drying, the sample was removed and weighed for mass balance calculations. A mass of 4.653g was recovered, giving the process an overall yield of 92.3%. The material was collected for

burst launches, SRI launches, and any future testing required. Launch data is reported below in Section 5.2.

4.3.1.2 Silica shelling

RCL-9 TiO_2 was shelled with a thin shell of silica by mixing TiO_2 particles with dilute tetraethyl orthosilicate in ammonia hydroxide and ethanol. RCL-9 and tetraethyl orthosilicate concentrations were swept to create a uniform shell and limit self-seeding. The coated materials were tested using a water/octanol partition test, which involves shaking equal parts water and octanol in a seperatory funnel with a small amount of sample, then letting the mix equilibrate overnight. After equilibration, a UV-vis is taken of both liquids, and the peak reading at 530 nm is used to determine relative concentrations. The partition coefficient K is determined by dividing the concentration in octanol over the concentration in water – therefore, a value of K <1 implies a more hydrophilic coating, while a value of K >1 implies a more lipophilic coating. This material is shown in **Figure 4.9.**

4.3.1.3 3-(Trimethoxysilyl)propyl methacrylate

Combined 5 grams of RCL-9 with 3-(Trimethoxysilyl)propyl methacrylate to create a hydrophobic shell. No noticeable shell evident in TEM image; however, the particles were dispersible in octanol during water/octanol partition. Using UV-vis, calculated K = 8.0. A LabRAM sonic wave vibrator was used to break up the pellet after centrifugation. The materials were concentrated to 25 mL in water and freeze dried. A TEM of this particle is shown in **Figure 4.10.**

4.3.1.4 Magnesium stearate and stearic acid

5 grams of RCL-9 was coated using magnesium stearate and stearic acid in organic solution. Very clearly went into octanol with K = 269. LabRAM was used to break up the pellet after centrifugation. Particles were concentrated to 25 mL in water and freeze dried. A TEM of this particle is shown in **Figure 4.11.**

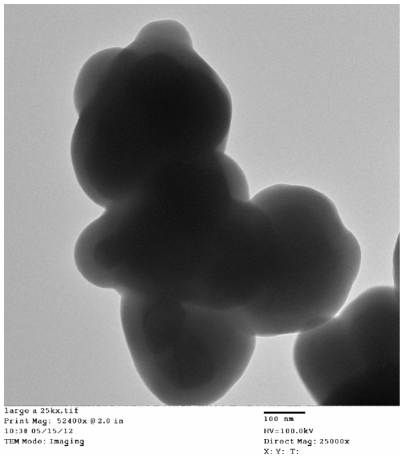

Figure 4.9: Silica shelled TiO_2.

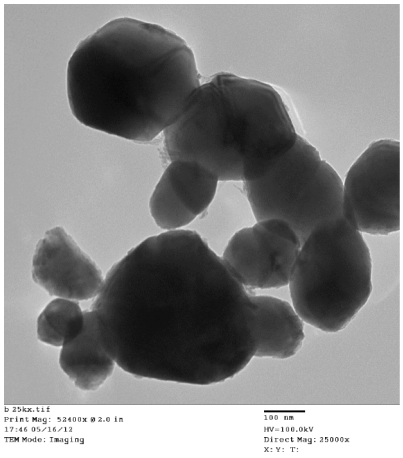

Figure 4.10: Titania nanoparticles after shelling with 3-(Trimethoxysilyl)propyl methacrylate.

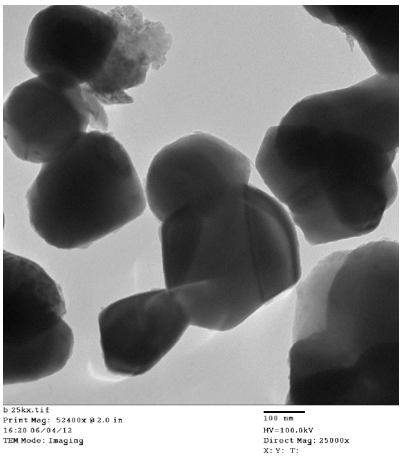

Figure 4.11: TiO_2 with magnesium stearate and stearic acid.

4.3.1.5 Acid reflux method

Another method to surface modify TiO_2 in solution is to treat the titania nanoparticles with hot sulfuric acid to activate the surface of the titania. After acid activation to form hydroxyl groups, the acid is removed using centrifugation and then the titania is exposed to a silane with appropriate functionality in toluene. The treatment with acid creates active hydroxyl groups on the surface of the titania. These functional groups then condense with the alkoxide functionality on the silane leaving the alkyl silane moiety covalently bound. Initial experiments to isolate the acid activated titania using tangential flow filtration proved challenging, with the material rapidly blocking the filtration media. More success was obtained with isolation of the activated titania by centrifugation. The large size of the particles makes centrifugation separation rapid and this method is scalable to multiple kilograms of material.

After isolation of the activated titania material by centrifugation TiO_2 particles were suspended in isopropanol or toluene, and refluxed at 120°C for 3 hours with 1 mL of aminopropyltrimethoxysilane (APTES), diphenyldimethoxysilane(DPDMS), octadecyl trimethoxysilane(ODTMS), pentafluorophenyltrimethoxy (PFPTMS) silane and perfluorooctyltrimethoxysilane (PFOTMS) (AXS1629, AXS1630). The APTES, DPDMS, and ODTMS will impart a hydrocarbon surface to the titania while the PFPTMS and PFOTMS will generate a perfluorinated surface.

After refluxing in toluene the titania, the particles were transferred to t-butanol and spray freeze dried (JCI0305). An image of the spray freeze dried powder coated with DPDMS is shown in **Figure 4.12**.

4.3.1.6 Solution milling of RCL-9

RCL-9 in an aqueous solution was milled using an attritor mill optimized for nanoparticles, (Kotobuki Industries, Ultra Apex Mill). This mill has been shown to separate agglomerated particles down to < 20 nm primary size (Yoden 2004). Visually, milling appears to have been very successful for this sample. In **Figure 4.13**, the left side is a 1% volume fraction RCL-9 in

Figure 4.12: Spray freeze dried DPDMS coated TiO_2.

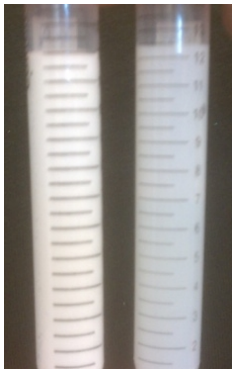

Figure 4.13: Left side is a 1% volume fraction RCL-9 in water sample without milling, while on the right is the same sample after 3 hours of milling.

water sample without milling, while on the right is the same sample after 3 hours of milling. The visible reduction in the amount of scattering is indicative of de-agglomeration of the sample.

4.3.2 Surface functionalization of RCL-9 TiO_2 as dry powder

TiO_2 surfaces exhibit low surface energy because of adsorbed hydrocarbons and carbonates from the ambient atmosphere. The surface is amenable to surface modification with compounds such as organosilanes. The surface modification can leave the surface either hydrophobic or hydrophilic, depending on the organosilane. The general formula for the silane is:

$$R_nSiX_{|4-„|}$$

R is an alkyl group and X is a hydrolyzable group

Surface functionalization experiments were performed to determine the impact of various organosilanes on dispersion. Four different silanes were tested: diphenyldimethoxysilane (DPDMS, Gelest), dimethyldimethoxysilane (DMDMS, Gelest), n-octyltrimethoxysilane (NOTMS, Sigma Aldrich), and hexamethyldimethoxysilane (HMDS, Sigma Aldrich). Coating was achieved using flask deposition and LabRAM deposition.

4.3.2.1 Fluidized Bed

Fluidized Bed Coater technology was used to coat both dried monodisperse silica nanoparticles and commercially available TiO_2. An advantage of the Fluidized Bed technology is that small (<100 g) samples can be coated which allows for the investigation of a greater variety of material than other techniques such as slant cone blender technology.

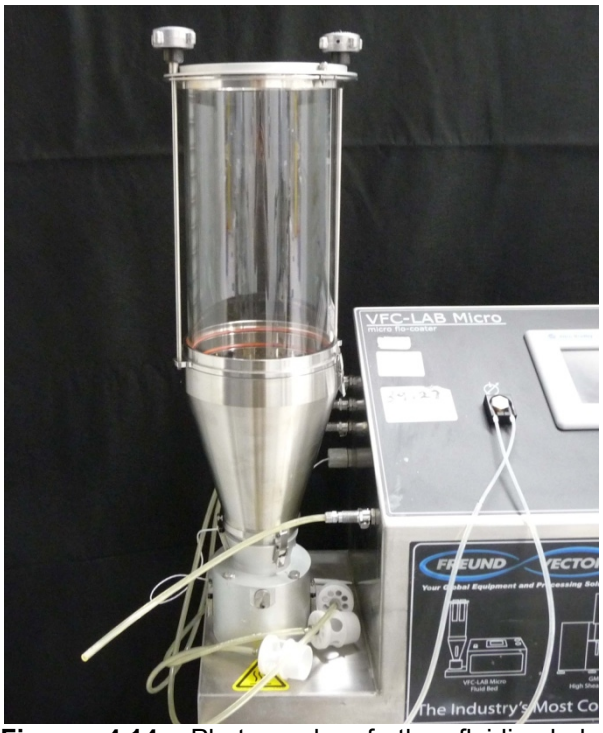

Figure 4.14: Photograph of the fluidized bed reaction chamber.

The fluidized bed reactor uses a stream of air from the bottom of the unit blowing up through a powdered solid such that the particles of the solid are in constant motion, supported on a bed of flowing air. The flow of air from the bottom balances the gravitation settling of the powder. The aerosolized particles can be evenly surface coated while minimizing aggregation. To surface coat the particles, a chemical is introduced via a spray apparatus. The fluidized bed employed by nanoComposix uses a porous bottom plate through which the suspending air flows and either a bottom mounted spray unit or a top mounted spray unit. The airflow can be heated such that additional surface coatings will rapidly vaporize rather than be discrete droplets. Material is prevented from leaving the chamber by the use of a filter on the air outlet. Clogging of the air outlet filter is reduced through the use of a pulsed back flow of air through the filter.

Two different configurations of a Freund Vector VFC-Lab Micro fluidized bed reactor were tried for the surface coating of titania nanoparticles with silanes. In the first the spray unit was located in the bottom of the sample chamber and was spraying up. In the second the spray unit was located at the top of the sample chamber and was spraying down.

Figure 4.14 gives a photo of the fluidized bed reactor. The reactor vessel consists of a cone shaped container with a porous bottom through which air can flow, a glass cylinder and a porous filter lid through which the air exhausts. **Figure 4.15** gives a photo of the inside of the spray chamber looking from above with the glass cylinder removed. In this figure the chamber is configured for bottom mount spraying with the spray head orientated such that the spray is angled up into the chamber.

For the bottom spray configuration a Wurster partition was used to allow a smaller sample size to be employed. The Wurster partition is a central tube through which the bulk of the airflow is directed. In theory, the powder should blow up through the central tube, meet the spray stream containing the surface coating and then fall to the outside of the tube before cycling through the center of the tube again. A range of different airflow conditions were tried in the bottom spray configuration using 50g of TiO_2 particles either P-25 aeroxide from Nippon chemicals or RCL-9 TiO_2. For both samples no conditions were found where the particles were suspended for more than about 15 seconds before they had bridged to the Wurster partition and stopped being fluidized. The particles had 'sand duned' into configurations such that the airflow no longer moved them. Attempting to spray when the particles were not moving was pointless.

Figure 4.16: Photograph of the fluidized bed reaction chamber from above with the glass cylinder removed in the top mount spray configuration where A is the spray head pointing down and B is the porous bottom plate.

For the top spray configuration a Wurster partition is not employed and the entire base of the sample chamber is porous and should not allow the 'sand duning' to occur (see **Figure 4.16**). 100g of RCL-9 $Ti0_2$ was loaded into the sample chamber. The material appeared to be well suspended for minutes at a time at the highest airflow setting with effective clearance from the exit filters through the use of regular pulsed air backflow. With the system in this configuration 1 mL of dimethoxydiphenylsilane was added through the sprayer over five minutes in 10 mL of ethanol. The air inflow was heated to 100°C. At the completion of the spraying the material was heated for a further 10 min in this configuration. The material had become substantially clumpier and the bulk of the material was adhered to the exit filters. No difference in surface contact angle was observed for a water droplet for material spread on a glass slide from the starting material. No difference in solubility in organic solvents was observed.

Figure 4.15: Photograph of the interior of the fluidized bed reaction chamber from above with the glass cylinder removed in the bottom spray mount configuration where C is the spray head passing through the bottom porous plate spraying up and D is the Wurster tube supported on three pins.

Consultation with the manufacturers of the fluidized bed suggested that the particle size of the titania particles was really too small for their machine, with 2 μm being the smallest they had employed and 50 μm being a much better size to employ. Also, it was suggested that particles with sharp edges rather than round balls tended to be less free flowing and thus not as good candidates for the fluidized bed.

The Fluidized Bed does not work well with individual particles in the 200 nm size regime. Changing the air flow direction and making other modifications was not successful. Therefore an alternate agitation method was used instead for TiO_2 powder coating.

4.3.2.2 Stirred flask and acoustic wave mixing

Silane coatings were applied to dry powdered Tiona RCL-9 TiO_2. Coatings were applied in a round bottom flask and also during an agitation process using a LabRAM acoustic wave mixer. The effectiveness of coating methods were evaluated by measuring the contact angle and ultimately the gFOM obscurant performance of packed powders.

4.3.2.3 Dimethyldimethoxy Silane

Dimethyldimethoxysilane (DMDMS) has the chemical structure shown in **Figure 4.17**. The silane has a density of 0.8638 g/cc and a boiling point of 82 ^{o}C. The alkyl groups will render the surface hydrophobic if coverage is complete.

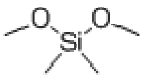

Figure 4.17: Chemical Structure DMDMS.

Initial experiments coated TiO_2 in a round bottom flask that was magnetically stirred. It was recognized that this is not an effective dissemination method and that this format may increase agglomeration. However, it provided a rapid method for determining whether the coating conditions were successful. Five grams of RCl-9 TiO_2 was magnetically stirred in a 3 neck flask (ambient room temperature) while nitrogen gas was used to transfer silane vapor from a second heated flask (82 °C)

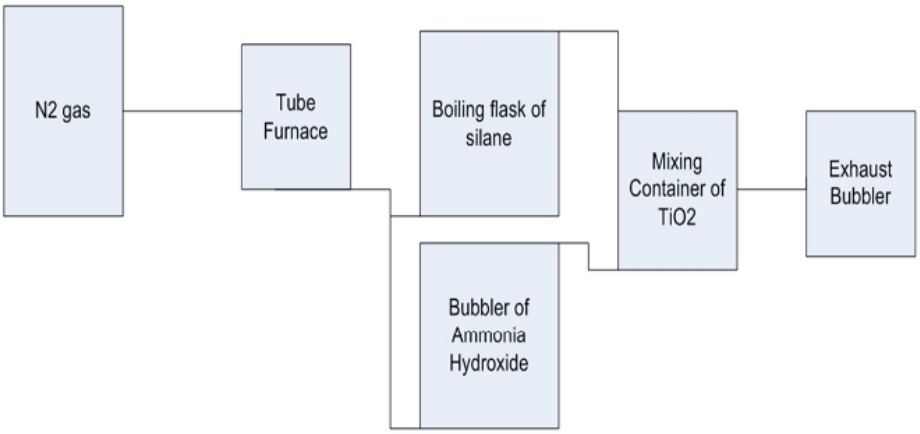

Figure 4.18: Schematic of flask deposition and LabRAM deposition setup.

containing ~5 mL of dimethyldimethoxy (DMDMS) silane. The third neck of the flask was connected to a bubbler that was used to monitor the flow rate of the transport gas that was set at 60 bubbles per minute (**Figures 4.18-19**). The experiment was run until the silane was almost completely vaporized, which took approximately 40 minutes. Half of a gram of TiO_2 was suspended in 10 mL hexane and water and then compared to uncoated TiO_2. Visually, the treated TiO_2 seemed to suspend better in hexane than water, indicating hydrophobic behavior. A slide of the treated TiO_2 was prepared by mixing the scintillation vial in the LabRAM acoustic mixer for 1 minute at

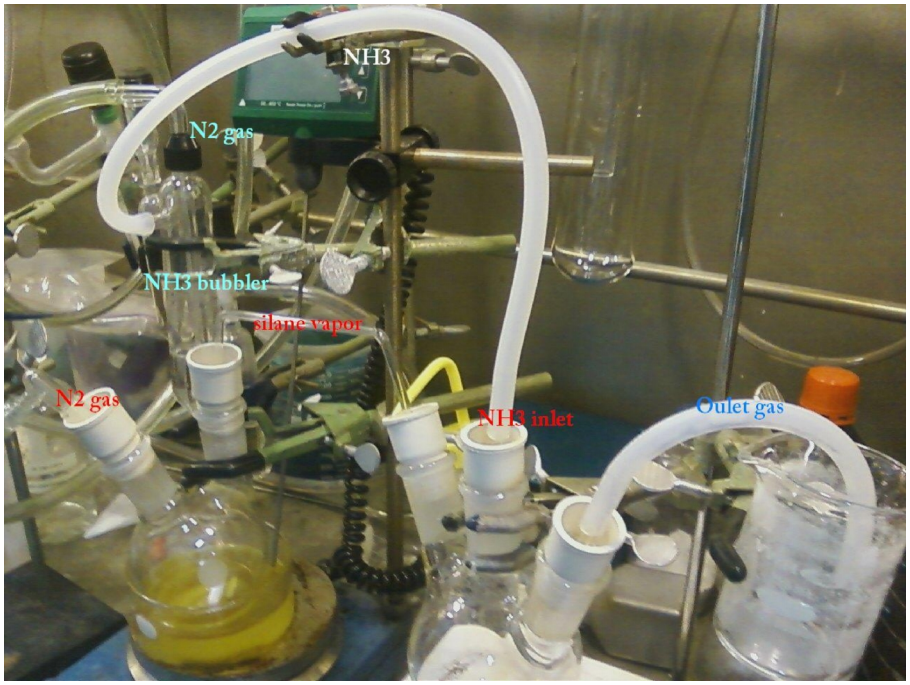

Figure 4.19: Setup for magnetic stir bar mixing for dual injected silane and ammonia. N_2 gas is fed into a bubbler of NH_3 as well as into the boiling flask of silane. The silane and NH_3 both run on separate lines, which lead into the inlets of the TiO_2 boiling flask.

approximately 50 G's. The mixture was then transferred via a 1 mL pipette onto a preheated slide. Despite suspending in hexane and being seemingly hydrophobic, the contact angle test did not verify any hydrophobicity, suggesting no surface incorporation had occurred.

A second set of experiments utilized the co-addition of NH_3 during the deposition process. Addition of ammonia to the gas stream promotes the base catalyzed condensation of the silane on the surface of the titania. The ammonia hydroxide was introduced by splitting the stream of N_2 transport gas using a plastic T-junction, with one stream going into the boiling flask of silane and the other to a bubbler of ammonia. The bubbler of ammonia hydroxide was set to approximately the same flow rate as the bubbler at the end of the line, which was controlled by using an adjustable clamp added onto the transport line going into the silane flask. Various timings were experimented with for the optimal time to introduce the ammonia. It was determined that the best process was to introduce the NH_3 slightly after the silane began to boil, injecting both the silane and strong base into the TiO_2 at the same time (**Table 4.1**). Based on these results, the dual injection of silane and ammonia was used in subsequent experiments for the functionalization of TiO_2.

Experiment	Contact Angle
No NH_3	0
NH_3 after silane	80
NH_3 & Silane	90

Table 4.1: Contact angle of surface functionalized TiO_2 according to the presence or absence of ammonia.

4.3.2.4 LabRAM Deposition

Magnetically stirring powder in a flask is not optimal for avoiding agglomeration since the powder is not suspended. Previous attempts to coat TiO_2 using a Fluidized Bed were not successful (Section 4.4.1). As an alternative, we used a LabRAM acoustic wave mixer from Resodyn to aerosolize the material during the coating process. The LabRAM mixes solids and liquids by vibrating at an appropriate resonant frequency generating very high accelerations (up to 100 Gs) over short distances.

Much like the flask deposition, N_2 was used as a transport gas, split with a plastic T-junction with one line going into the two neck silane boiling flask and the other going into the bubbler of ammonia hydroxide. The oil bath for the silane boiling flask was set to 92 ^{o}C. The lines transporting the gas were made of platinum coated silicon, which is heat and chemical resistant. The outlet lines of the silane flask and the ammonia hydroxide bubbler then met at another plastic Tee and went into a 60 mL plastic bottle with plastic barbs tapped into the bottle walls. Using an equivalent procedure to that employed for the stirred flask coating, the contact angle went from 90 degrees to 120 degrees, showing an increase in hydrophobicity. Furthermore, SRI testing of loose powders showed a yield percentage increase from 25% on average to 55%. The LabRAM then became the focus for small scale testing.

4.3.2.4.1 N-octyltrimethoxy Silane (NOTMS)

The next silane investigated with the LabRAM was N-octyltrimethoxy silane (NOTMS) due to its lower boiling point (191.5 °C). Due to condensation of the silane in the transport tubing, it was necessary to reduce the length of the tubing and to pre-heat the carrier gas. Testing various silanes in order to determine which silane is the most optimal for surface functionalization is an important facet to our research. NOTMS was of interest due to its trimethoxy group and a boiling point between DMDMS and DPDMS (191.5 °C). First experiments performed with the magnetic stir bar method but were not successful due to the silane vapor condensing in the lines and being introduced as a liquid into the TiO_2. Shortening the path length between the boiling flasks aided in reducing condensation, but it wasn't sufficient to prevent condensation. It was then necessary to preheat the transport gas, so that the lines were at the boiling temperature of the silane. The set-up for the deposition is described in the sections below.

Tube Furnace

A tube furnace was used to pre-heat the carrier gas. 7.6 meters of copper tubing were coiled to fit inside the tube furnace. The tube furnace was angled at 45°, such that the heated N_2 gas outlet was at the same level as the boiling flask of silane. The furnace temperature was set to 240 °C to reduce the effect of thermal degradation as it pertains to the condensation of the silane vapor. To minimize condensation of the silane vapor is it important to keep the length of the lines in between the tube furnace, the boiling flask of silane, and the container of TiO_2 as short as possible.

Silane boiling flask and NH_3 bubbler

Silane Flask

Preheated N_2 runs from the copper coil inside the tube furnace to the inlet of the tee junction tube Swagelok. One outlet is connected to an inch long piece of ¼" outer diameter (OD) copper tubing, insulated with aluminum foil. A two inch piece of platinum coated tubing connects the furnace outlet to another piece of copper tubing attached to the inlet of the boiling flask. The platinum coated tubing is used due to its flexibility and because it can be clamped to reduce the flow of N_2 into the boiling flask of silane. The heating mantle underneath the boiling flask was set to 220 ^oC. The heating mantle is set to this temperature to ensure that any silane vapor in the boiling flask will be well above the boiling point of the n-octyl silane, to decrease the probability of condensing in the lines.

First attempts of this experimental set-up utilized copper tubing that ran out of the outlet of the boiling flask of silane. The copper tubing was initially used, because it was thought that it would hold heat from the N_2 as the gas passed over it, and if properly insulated, would keep the system at the desired temperature with minimal thermal degradation. The problem with this set-up was that the copper, although wrapped with foil, was still cooling and condensing the gas. Switching to a glass connector improved the insulation and facilitated the return of condensed silane back to the boiling flask. Having a steep angle connector is also important because it increases the probability of any condensed silane vapor returning to the boiling flask and not into the container of TiO_2. After the glass connector, another piece of platinum coated tubing was used to connect the glass to the container of TiO_2. This was done to allow flexibility when the LabRAM was in use. A simple hose-tie was used to hold the glass to the platinum coated tubing.

NH_3 bubbler

The other outlet from the furnace gas was connected to platinum coated tubing and then into the inlet of the NH_3 bubbler. It is not necessary to have the bubbler of NH_3 be as heated as the silane vapor, because only a small amount of the ammonia is flowing into the container of TiO_2. The outlet of the ammonia bubbler has a piece of platinum coated tubing for flexibility that then runs to a piece of copper tubing, and then another small piece of platinum coated tubing is used to connect the copper to the container of TiO_2 (again, for flexibility, when the LabRAM is in use). The NH_3 was "turned on" after the TiO_2 had been exposed to the silane for 10 minutes. The ammonia bubbler was set to approximately 1 bps or "bubbles per second." The bubbler of distilled water at the end of the line was set to approximately 6 bps.

LabRAM

5 grams of TiO_2 were loaded in a 125 mL polycarbonate vessel with two inputs from NH_3 and silane and one exhaust. The LabRAM was set to increase mixing intensity in increments. Upon the heating mantle and tube furnace reaching their set temperatures, the LabRAM was turned on. The intensity levels went from 10%, to 15%, to 25%, and to 30% at time 0, 20 min, 40 min, and 50 min respectively. The intensity levels were varied over the experiment because the TiO_2 settled at an intensity level if it remained in that state for too long. The variation of intensity created an improved TiO_2 aerosol. The entire process lasted 60 minutes. Stir bar prepared films had a contact angle of 140 degrees, well above the DMDMS results. LabRAM deposition using the set-up shown in **Figure 4.20** were successful and also produced thin films with contact angles >140 degrees.

4.3.2.4.2 Diphenyldimethoxy Silane

The DPDMS was the primary silane of interest, due to its previous success in increasing the yield and extinction data when used by ECBC to coat TiO_2 [DeLacy 2011]. The progression for experimenting with DPDMS is much the same as with the NOTMS. Due to the exceptionally high boiling point of the silane (286 °C), additional attention to monitoring flow rates, temperature fluctuations with the heating mantle and tube furnace, and other sources for thermal degradation was required.

The first step to coating TiO_2 with DPDMS was to get a successful result with the stir bar method. Using the same stir bar method as with the NOTMS, we were able to get a contact θ=150 degrees, slightly larger than the NOTMS with the same testing parameters. After a successful result with stir bar mixing, the experiment was moved to the LabRAM. After multiple experiments, augmenting small components of the setup in order to debug the process, we were able to coat TiO_2 with DPDMS in the LabRAM (**Figure 4.20**). The experiment yielded a contact angle of >140 degrees, slightly higher than that of the NOTMS.

4.3.2.5 Scale up of Trimethoxy(octyl)silane coatings

Initial experiments have shown that a LabRAM Acoustic Mixer can be successfully employed to coat from 50 – 240 grams of TiO_2 at a time. However, this initial system was fairly limited in temperature, pressure, and flow rate control. The lack of control resulted in batch to batch variations in coatings. A completely revamped system with additional thermocouples, heating mantles, and valves was created in order to solve these outstanding issues. The reaction chamber used in the LabRAM was refitted with Teflon through-wall Swage-lok fittings to reduce the overall weight from 250 grams to only 214 grams; this allows for more TiO_2 to be coated at a time given the max 500 gram load of the LabRAM. Stainless steel tubing and valves were also

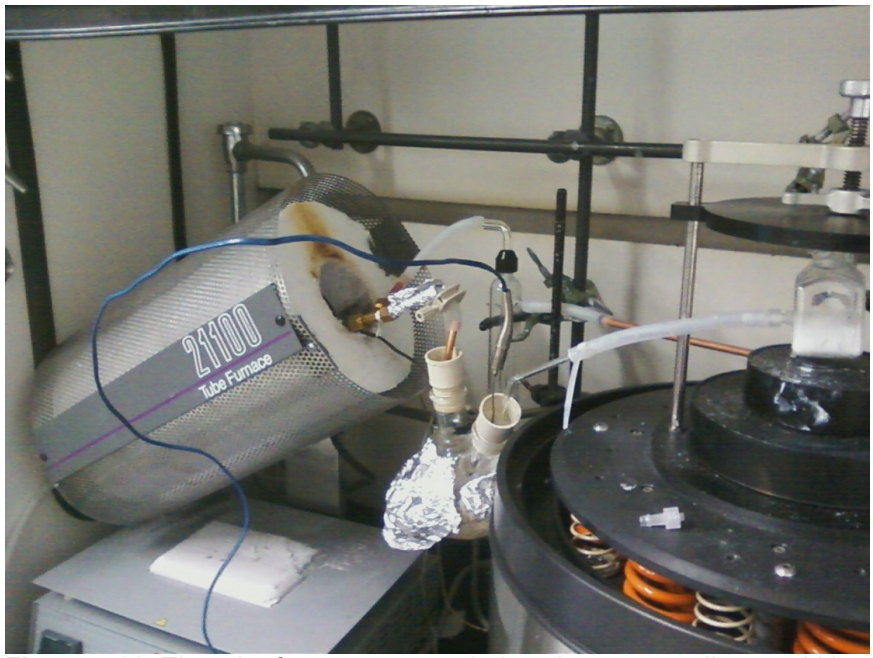

Figure 4.20: The tube furnace was angled so that no extra line would be used to get the preheated N_2 into the boiling flask of silane. The preheated N2 then ran into a Swagelok, which acted as a T-intersection, with one outlet running to the bubbler of NH_3 and one outlet running into the boiling flask of silane. The boiling flask of silane outlet then ran into a glass connector with a steep angle around 15 degrees with the y-axis, in hopes that any silane vapor that condensed in the tube would fall back down into the boiling flask, leaving only vapor to enter the mixing container in the LabRAM.

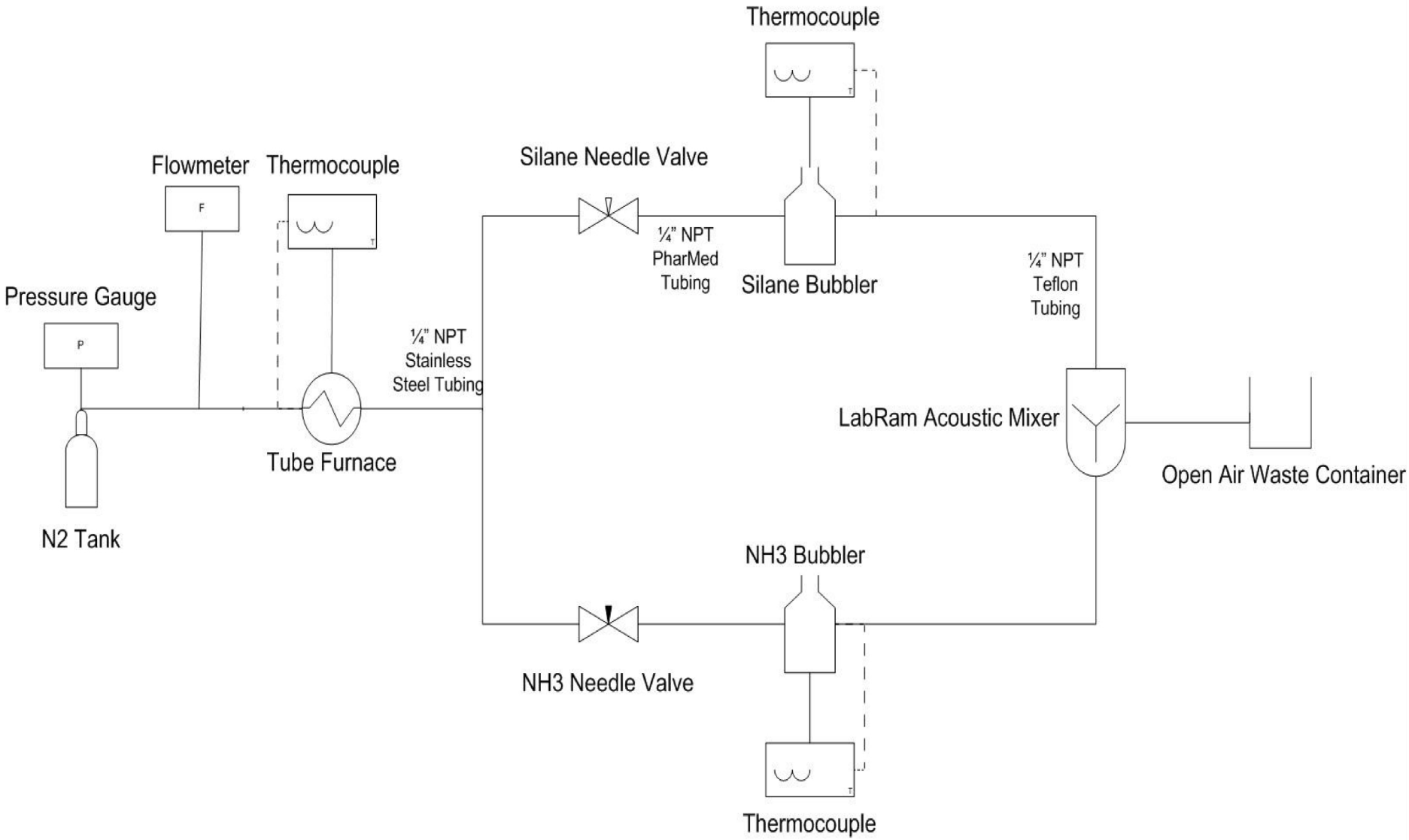

Figure 4.21: Schematic of system used to successfully coat TiO_2.

used to reduce the overall heat loss of the gases while providing flow rate control for the system. An advantage of this system is that it is reliable and provides consistent results batch to batch, which suggests the possibility of future scale up to 280 grams batches.

The system heats selected silanes (e.g. Trimethoxy(octyl)silane, NOTMS) to 10-15 ºC above its boiling point in a flask and then carrying the vapor with superheated N_2 gas (250-350 ºC) into the reaction chamber. This reaction is base catalyzed in the presence of ammonia vapor, which is also carried into the chamber with superheated N_2 gas. The TiO_2 within the reaction chamber was vigorously shaken at 40-50 Gs to maximize the overall surface area of TiO_2 particles for an optimal coating. **Figure 4.21** shows a schematic for the entire system.

The reaction chamber employed a pint sized aluminum paint can fitted with three ¼" NPT Teflon Swage-lok fittings to minimize heat loss and weight. ¼" NPT Teflon/PTFE hollow caps were drilled with a $^1/_{16}$" bit and attached inside the can to the Teflon bulkhead fitting. The cap served as a flow restriction, accelerating the N_2 gas velocity and minimizing the backflow of TiO_2 into the silane and ammonia flasks. **Figure 4.22** shows the actual coating chamber while **Figure 4.23** is an image of the running system used to successfully coat TiO_2 powders.

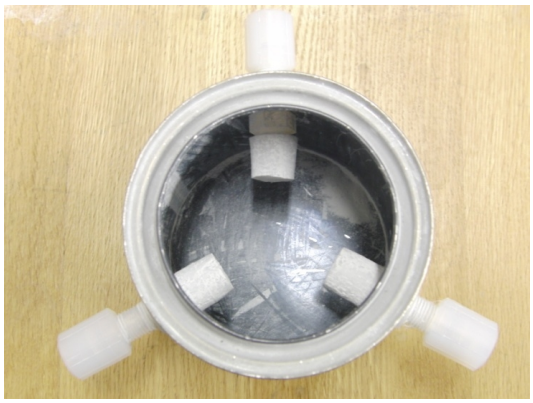

Figure 4.22: Custom made reaction chamber.

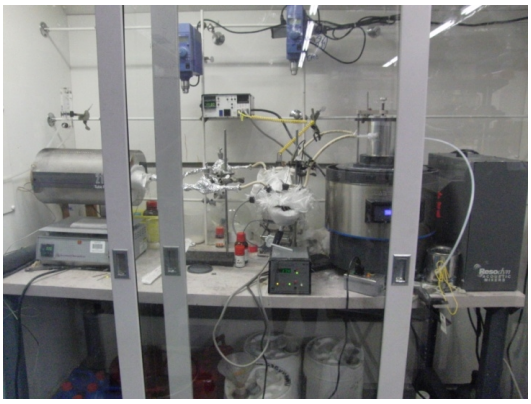

Figure 4.23: Image of running system.

A tube furnace (Barnstead, Thermolyne F21135) was set up with a 7.6 meter coil of ¼" copper tubing surrounded by fiberglass cloth insulation and attached to the stainless steel tubing with a double Swage-lok coupler. The stainless steel valves were also insulated with fiberglass while the stainless steel tubing was surrounded by a thin layer of aluminum foil to minimize convective heat loss in the fume hood. These valves were attached to hollow rubber stoppers drilled with 1/8" holes to accommodate hollow glass cylinders which extended into the boiler flasks. The silane and ammonia were contained in two, three necked 250 mL and 100 mL flasks, respectively. They were surrounded by a few layers of fiberglass insulation and placed on top of a heating mantle. The inlet glass cylinders extended far into the flask touching the bottom while the outlet glass cylinders were placed such that they extended only a few inches from the stopper and not touching the liquid. The stainless steel tubes from the valves were attached to the glass tubing with ¼" PharMed tubing and secured with metal hose clamps. The outlet from the flask was attached with ¼" PharMed tubing with hose clamps and secured to ¼" Teflon tubing going into the coating chamber with shrink ties. Thermocouples were fitted into stoppers such that the tips were immersed in liquid to give the most accurate readings.

The initial setup was connected to two flow meters instead of the reaction chamber to do a pressure and flow rate calibration. Each valve was partially opened with one full turn each. The most optimal N_2 pressure was found to be roughly 10 psi to minimize the failure of the stoppers and give maximal flow rate control. The overall flow rate, before the tube furnace, was set anywhere from 3.5 – 4 LPM which read a corresponding 1.5 – 2 LPM for each individual valve. After this initial calibration, the entire system was connected and prepared for a run.

The temperature on the tube furnace was set at 300 ºC, with a ramping rate of 6 ºC/min and left to preheat for roughly 20 minutes before heating up the reagents. The maximum temperature of the furnace is roughly 400-500 ºC; however, this was not ideal as it tended to overshoot 50 to 100 ºC during runs. The set point of the silane was 210 ºC instead of the 191.5 ºC boiling point at atmospheric conditions. A variety of silanes with boiling points under the 250 ºC threshold of the heating mantle can be used in this setup. It took roughly 15 minutes to reach the boiling point of the silane. The 30% ammonia hydroxide solution was set to heat up to 100 ºC and vaporized very quickly within 5 minutes.

The valves were partially opened one full turn while the primary flow meter was closed off until the reagents were ready. The vaporization of silane was the most important part of the system, so a heat gun was applied to the flask until there was visible vapor within the flask before the N_2 was turned on. The tubing and valves were heated with the heat gun to minimize the thermal loss created by the valves functioning as heat sinks. Once everything reached the set temperature, the LabRAM was turned on to 50% intensity and 50 Gs and the flow meter was opened to 3.5-4 LPM and left to run for approximately 15-25 minutes or until all of the silane was gone. This flow rate was found to give a fast coating time of only 15-25 minutes instead of the previous 1.5 to 2 hours.

Various amounts and ratios of reagents were attempted (**Table 4.2**), but it was found that 50 gram batches were made most successfully in a 5 to 1 ratio of mL silane to gram TiO_2. The amounts of reagents used which arguably gave the best results were: 50 grams RCL-9 TiO_2, 10 mL silane, and 25 mL ammonia.

A simple initial qualitative test of hydrophobicity was conducted after each run (PQ0012 – PQ0023), using approximately 0.5 grams of sample and 15 mL hexane in a glass scintillation vial. The vials were vortexed and sonicated until the powder appeared to suspend within solution. Hydrophobic powders clearly suspended for long periods of time within the hexane and turned the solution a milky white. Our best mode functionalized powder suspended for greater than 10 minutes, depending on the mixing mechanism. This served as the standard for determining the relative hydrophobicity from batch to batch. Poorly coated powders or the control RCL-9 fell out of solution almost immediately even with vigorous agitation, indicating a lack of a hydrophobic coating.

Sample ID	Silane	Mass TiO2 (g)	Silane (mL)	Ammonia Hydroxide (mL)	Grams TiO_2 / mL Silane
PQ0012	NOTMS	50	25	60	2
PQ0013	NOTMS	100	10	60	10
PQ0014	NOTMS	100	19	60	5
PQ0015	DPDMS	50	10	50	5
PQ0016	NOTMS	100	25	50	4
PQ0017	NOTMS	50	12.5	25	4
PQ0018	NOTMS	50	12.5	50	4
PQ0019	NOTMS	50	12.5	50	4
PQ0020	NOTMS	50	10	25	5
PQ0021	NOTMS	50	10	25	5
PQ0022	NOTMS	50	10	25	5
PQ0023	NOTMS	50	10	25	5

Table 4.2: Summary of reaction conditions for scaled up dry powder surface modifications using the LabRAM mixer. Samples 19 – 23 were combined to form a master batch for field testing.

5 Results and Discussion

Surface modified materials were evaluated as a bulk powder by measuring the hydrophobicity via contact angle, water / octanol partitioning, and as an aerosol launched as a powder compressed into a packed device.

5.1 Evaluation of surface functionalized TiO_2 powders

5.1.1 Small batches (5 grams)

5.1.1.1 Contact Angle

Contact angle measurements are summarized in **Table 5.1**. NOTMS and DPDMS coatings had contact angles >140 degrees for both stir bar mixing and LabRAM mixing. These contact angles surpassed those obtained from solution coatings (**Table 5.2**) using other silanes in Section 4.3.1.5.

Silane	Mixing Method	Contact Angle
DMDMS	Stir Bar	90
NOTMS	Stir Bar	140
DPDMS	Stir Bar	150
DMDMS	LabRAM	120
NOTMS	LabRAM	>140
DPDMS	LabRAM	>140
DPDMS	DeLacy(Slant Cone)	137.2
NOTMS	DeLacy(Slant Cone)	147.1

Table 5.1: Contact angle measurements of surface modified TiO_2 using a variety of mixing methods.

5.1.2 Scaled up batches (50 grams)

5.1.2.1 Octanol-Water Partitioning

An octanol-water partitioning test was performed on the samples to create a quantitative model of the hydrophobicity of the TiO_2. 10 mL of 1-octanol, 10 mL of DI water, and 10 mg of TiO_2 were placed into 60 to 125 mL separation flasks. These flasks were well shaken and left to sit overnight for the samples to settle. **Figure 5.1** shows an image of how the certain powders behaved in this test setup. The uncoated control and poorly coated (PQ0013) clearly suspended in the water while the octanol partition only appeared white due to coating of the glass interior by the TiO_2. The hydrophobic master batch (combination of multiple batches) suspended in only octanol, which was expected. The partially functionalized PQ0014 appeared to suspend in octanol but fell out directly into the liquid-liquid interface rather than fully

Silane Group	**Contact Angle**
Pentaflurophenyl-trimethoxysilane	124°
Diphenyldimethoxy silane	N/A (Wetting effect)
Perflurooctyl triethoxysilane	130°
Octadecyl trimethoxysilane	130°
Aminopropyl triethoxysilane	N/A

Table 5.2: Contact angle measurements of solution based surface modified TiO_2 .

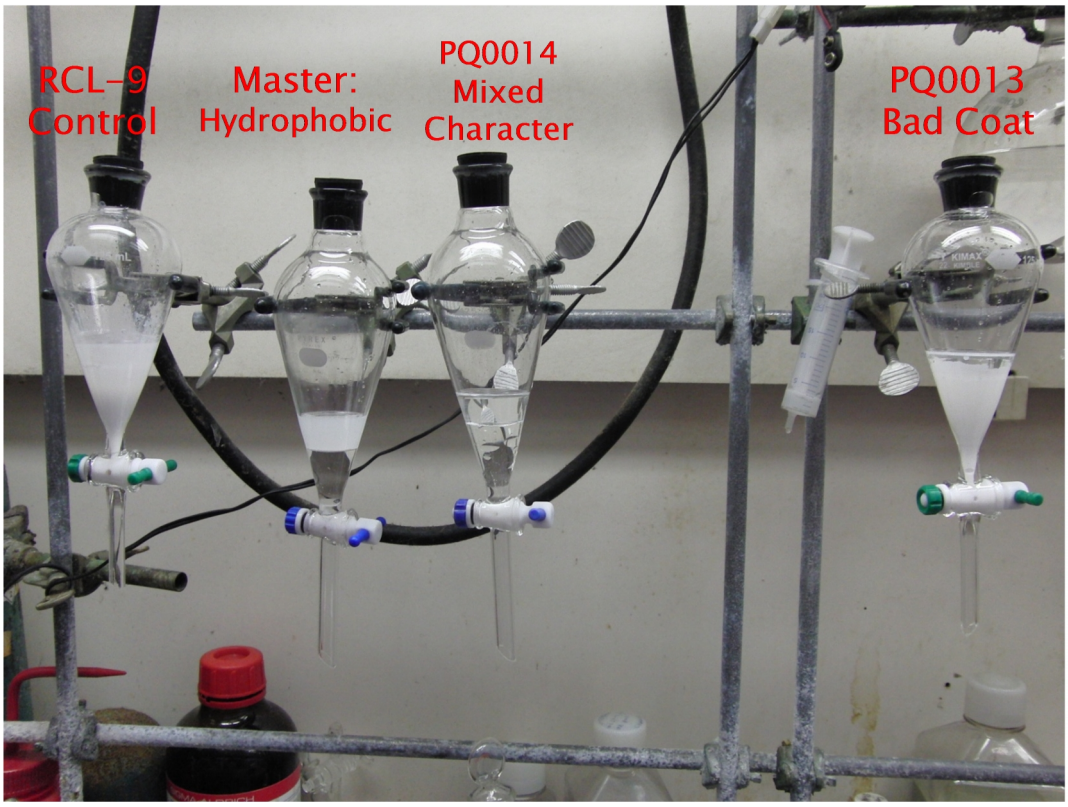

Figure 5.1: TiO_2 powders in octanol-water partitioning test.

suspend in either partition. This behavior is indicative of some weak hydrophobic character that prevents the particles from falling completely into the water below.

After taking aliquots of each partition in separate glass scintillation vials, the samples were diluted down in its respective solvent until the 480 nm wavelength read an absorbance within 0.2 to 1.0. Each sample in water was diluted down to the same factor as its complementary sample in octanol to give a base of comparison between the two. The maximum absorbance of each sample was used to normalize the rest of the readings so that the different dilution factors would be a non issue during analysis. The following figures document the data obtained from the UV-Vis spectroscopy of the samples.

Figure 5.2 shows that the coated TiO_2 behaved as expected with the control (RCL-9) and poorly coated samples (PQ0013) having a significantly higher peak absorbance in water than the hydrophobic samples. This meant that these samples were hydrophilic as most of the TiO_2 was partitioned in water rather than octanol. There appeared to be a broad peak around 550 nm, but a tapering off over the rest of the spectrum. For the hydrophobic samples, the absorbances were very low, wavering near a zero absorbance over the wavelength range.

Figure 5.3 confirms the hydrophobicity of the well coated powders, as the best modes, PQ0019-PQ0023, had the highest peaks and were significantly greater than the control and poorly coated powders when suspended in octanol. The peaks of the curves are not all at the same wavelength, with samples having a peak wavelength between 470 nm and 560 nm. The partition coefficient, K_{ow}, was calculated by determining the wavelength at which TiO_2 had a distinct peak and using the

absorbance at this wavelength as the max. The max absorbance for the sample in octanol would then be divided by the max absorbance in water to yield a partition coefficient. The range for which the max absorbance had to fall under was greater than 0 but less than 1.5 and for only a wavelength greater 350 nm.

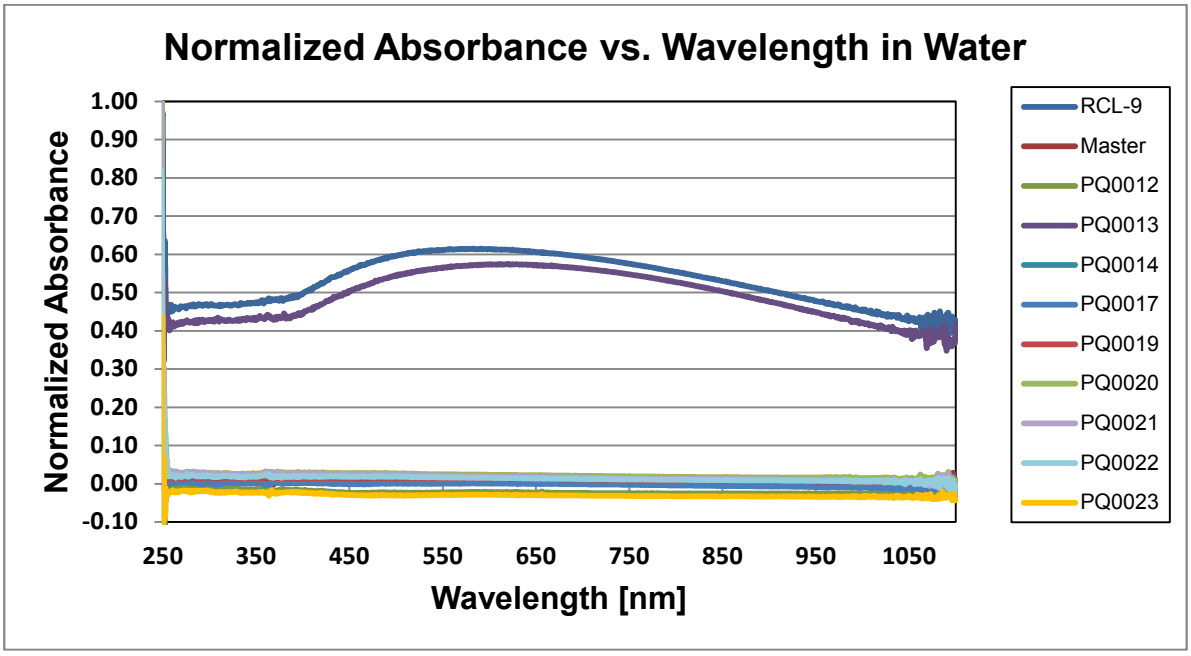

Figure 5.2: Normalized absorbances of the samples in water.

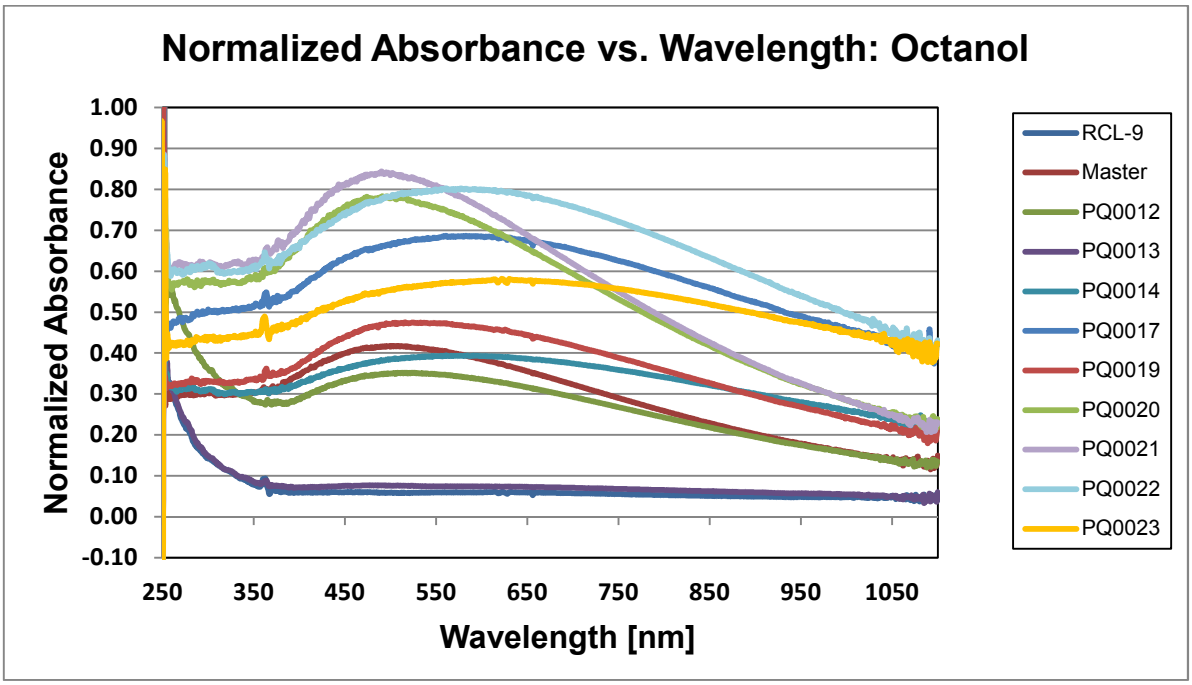

Figure 5.3 Noramlized absorbance of the samples in octanol.

Sample	Max Abs. Water	Max Abs. Octanol	K_{ow}
RCL-9	0.621	0.098	0.16
Master	0.033	0.470	14.24
PQ0012	0.000	0.495	-
PQ0013	0.519	0.131	0.25
PQ0014	0.026	0.456	17.54
PQ0015	0.919	0.276	0.30
PQ0017	0.006	0.776	129.33
PQ0019	0.027	0.500	18.52
PQ0020	0.033	0.087	2.62
PQ0021	0.029	0.943	32.52
PQ0022	0.028	0.950	33.93
PQ0023	0.000	0.586	-

Table 5.3: Summary of the calculated water octanol partition coefficients.

Table 5.3 is a summary table of the calculated partition coefficients. PQ0012 and PQ0023 had a zero value in the absorption in water and a K_{OW} could not be calculated. Ultimately, all of the hydrophobic powders still had a K_{OW} greater than one as expected; the control and best modes will serve as standards in future experiments.

5.1.2.2 **TEM Imaging**

For TEM imaging, 0.1 grams of the control and best mode PQ0023 batches were added to 10 mL isopropyl alcohol and sonicated for about 2 minutes. Then 4 μL of each sample were added to each TEM grid and left in a vacuum until dry. There appeared to be an interesting difference between the uncoated and coated particles at a low magnification in **Figures 5.4a** and **5.4b**, respectively. The control did not have any visible agglomeration of the same degree as the coated sample, which is exemplified by the large visible aggregates in **5.4b.** The magnification level was increased to 3000X as shown in **Figures 5.4c** and **5.4d**. Once again, there appeared to be significant aggregation in the coated sample that was not apparent in the control. It was speculated that this behavior was due to the drying methods employed; however, both samples were subjected to the same procedures and at the same concentrations. If drying were an issue, then both samples should have shown similar problems due to the consistency in procedures. Given that drying was not relevant, the agglomeration may have been caused by the coating itself. Multiple images of the samples in different grids were taken, yet they all appeared to have the same behavior as shown in these representative images.

Multiple images at 3000X were analyzed using ImageJ to determine the particle size and an average of these throughputs were taken as the average particle size for these samples. The control had an average diameter of 254.2 ± 68.5 nm while the coated batch had a diameter of 281.4 ± 52.5 nm.

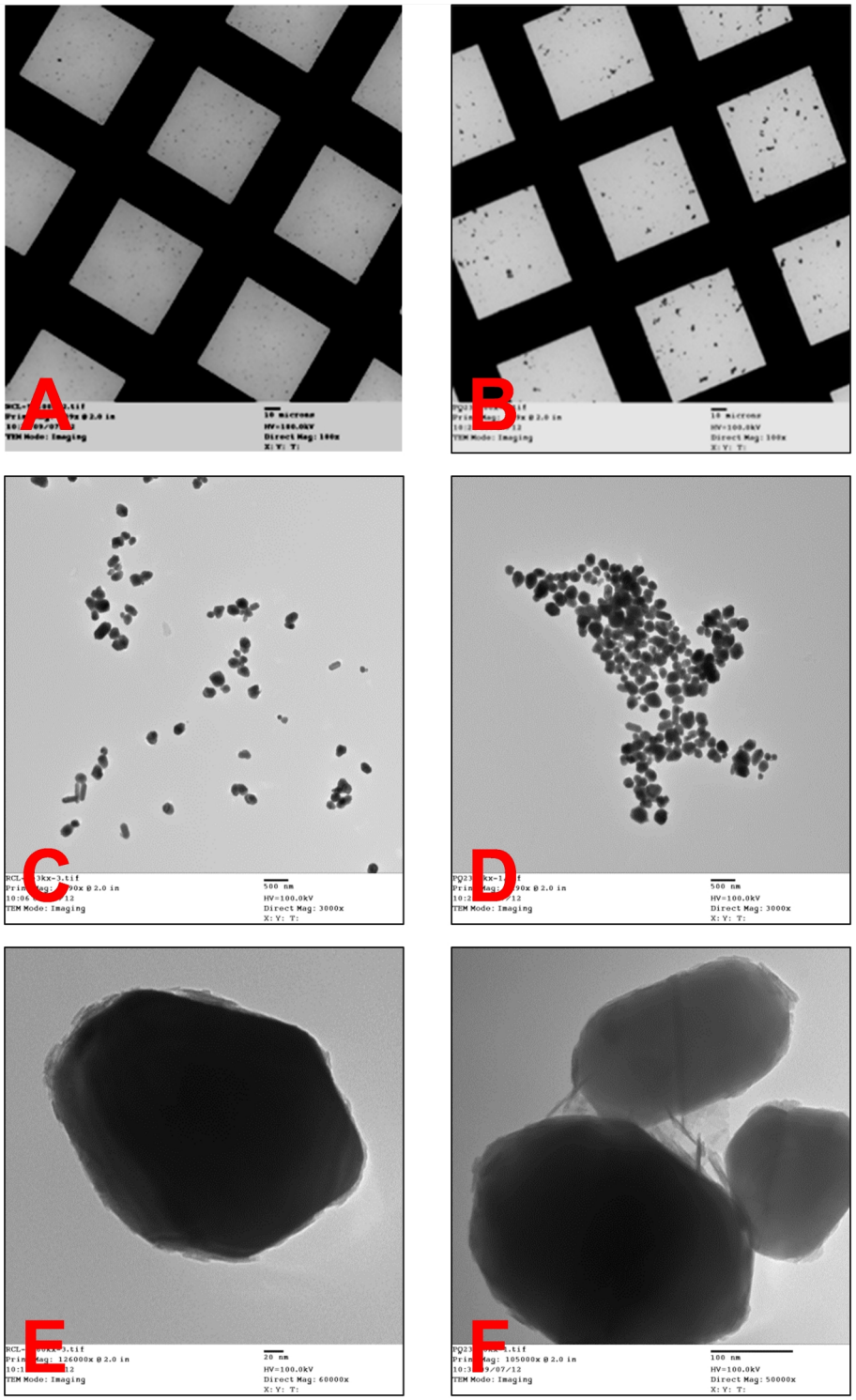

Figure 5.4: TEM images of control (Column 1) and best mode PQ0023 (Column 2) at 100X (Row 1), 3000X (Row 2), and 50,000X (Row 3).

Images were taken at a higher magnification (50,000X) to see if there was any detectable layer of silane on the coated particles as shown in **Figures 5.4e** and **5.4f**. An individual particle with roughly the same diameter was chosen from each sample and imaged at maximum magnification. Initially, the coated sample appeared to have some layer of material coating the outside of the particle; this behavior was prevalent throughout most of the other images taken for this sample. Upon closer inspection, the control also appeared to have some of the same coating on multiple particles. It is difficult to determine whether or not this layer is composed of silane or just due to the manufacturing process of the TiO_2 itself since both the control and coated sample have it. It is arguable that the particles of the coated sample are interconnected by a web of this unknown material. However, a higher resolution TEM or SEM is needed to detect any possible monolayers or bilayers on the coated samples.

5.1.2.3 **Contact Angle Measurements**

Contact angle measurements were made to provide another quantitative measure of hydrophobicity of the most representative samples (control, master, PQ0022, PQ0023). A camera was mounted in front of a slide stage, which was covered by a box to reduce ambient light pollution. A light diffuser was placed on the end of the box in front of a light source to give even lighting.

Sample preparation required 0.5 grams of sample in 5 mL of the best solvent (water for hydrophilic and hexane for hydrophobic). These samples were sonicated and 1 mL of each was pipetted onto heated glass slides and baked in the oven until dry. 5 µL of water was dropped onto each slide and placed onto the imaging platform. Super macro images were taken of each droplet and analyzed using two readily available and well documented ImageJ scripts: *Dropsnake* and *Contact Angle*. *Dropsnake* uses a B-spline snake with active contours that has no shape assumption, which is able to give both a left and right contact angle. *Contact Angle* uses a spherical and elliptical approximation, giving an overall contact angle measurement. The averages of both results of duplicate slides were taken as the contact angle of the sample. **Figure 5.5** shows an example of the contact angle calculation for the best mode PQ0023.

The very poorly coated powders did not have enough hydrophobic character for a significant bead of water to form for contact angle measurement. **Figure 5.6** shows the clear lack of hydrophobicity of the control sample in comparison to **Figure 5.5**.

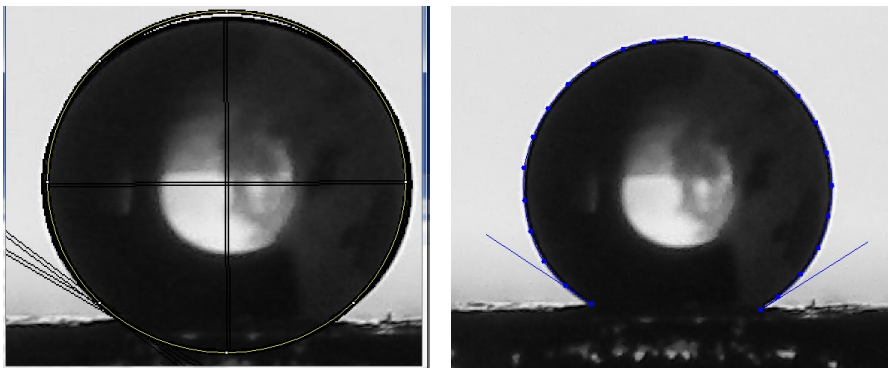

Figure 5.5: Contact angle measurements using *DropSnake* (left) and *Contact Angle* (right).

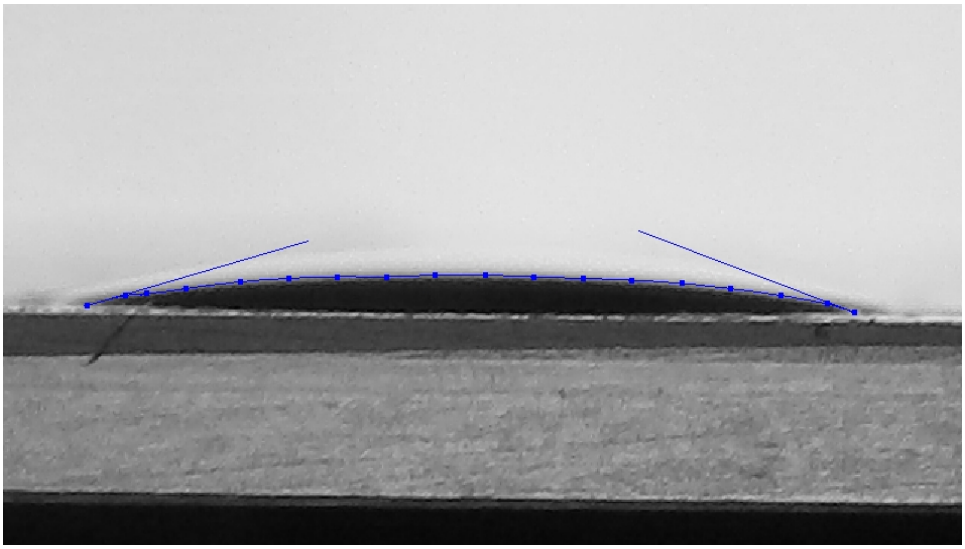

Figure 5.6: Contact angle measurement of RCL-9 control.

Table 5.4 is a summary table of the contact angles for the master batch, two best mode samples, and the RCL-9 control. Clearly, the hydrophobic powders have a significantly higher contact angle than the control. Note the high CV of the control, which was caused by an uneven wetting of the surface due to its hydrophilic nature.

Sample	Contact Angle	CV
RCL-9	16.6	13.0%
Master	104.5	2.6%
PQ0022	128.2	1.8%
PQ0023	140.9	5.0%

Table 5.4: Summary table of contact angles.

Both Zeta Potential and Disc Centrifuge measurements were also taken of the different coated TiO_2 samples. High quality data could not be obtained for the hydrophobic polymers due to the nature of the instrument methods and their incompatibility with hydrophobic solvents.

The LabRAM setup worked very well in applying a hydrophobic coating to batches scaled from 5 grams to 50 grams of TiO_2. This system was consistent and reproducible with the final five batches running without a hitch and all with excellent hydrophobic characteristics. The hydrophobic powders behaved as predicted in an octanol-water partitioning test and yielded high contact angles of 128 – 140 degrees in comparison to the control (17 degrees).

5.2 NCX Chamber testing

Surface modified TiO_2 powders were evaluated in the 2.5 m^3 aerosol test chamber, launched in packed formats. Comparisons were made to unfunctionalized powders to determine the improvement over the baseline material.

5.2.1 Evaluation as packed powder

5.2.1.1 1 mL, 1 gram format

Surface modified powders were evaluated at nanoComposix to determine the yields, fill fraction, MEC and gFOM (**Table 5.5**). Surface modified powders were packed into a fixed volume device and a load applied to maximize the fill fraction without degrading the extinction and yield. 500 psi was found to be an optimal compression pressure for TiO_2. 1 gram samples were compressed to 500 psi in a 1 mL PDD format (**Figure 5.7, right**) and launched with a high pressure reduced gas volume solenoid valve system (**Figure 5.8**). Best mode in this format was found with N-OTMS coated material giving a yield of 60% and gFOM of 1.91 m^2/cm^3.

Format	Material	Coating Method	Pressure (psi)	Fill Fraction	Yield	MEC (m^2/g)	gFOM (m^2/cm^3)
1mL	RCL-9	n/a	500	0.34	0.50	1.21	0.85
1mL	Tiona 188	n/a	500	0.42	0.48	1.92	1.60
1mL	DeLacy RCL-9 DPDMS	Slant cone	500	0.36	0.47	1.92	1.36
1mL	RCL-9 n-OTMS (JRE1024)	LabRAM	500	0.41	0.60	1.87	1.91
1mL	RCL-9 DPDMS (JRE1025)	LabRAM	500	0.35	0.18	1.59	0.39

Table 5.5: TiO_2 powders packed into 1 gram, 1 mL PDD format and evaluated in NCX 2.5 m^3 aerosol chamber.

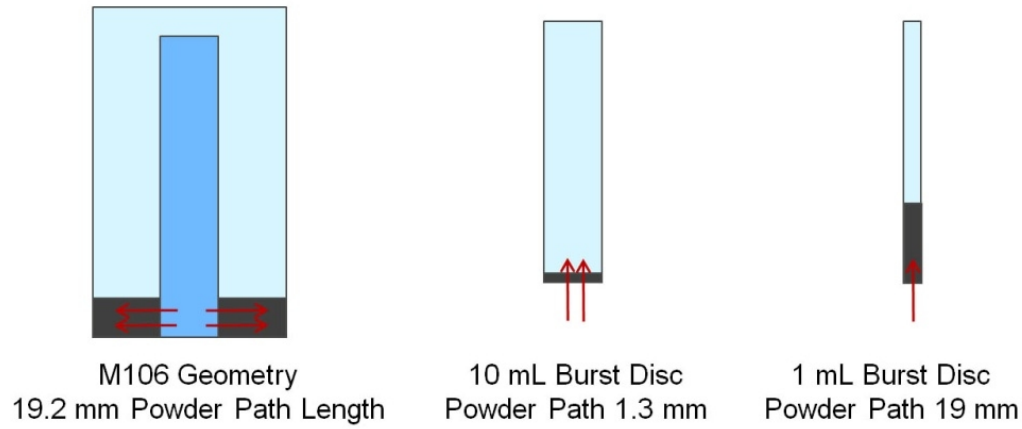

Figure 5.7 Packed device geometries.

We have successfully coated 5 gram batches TiO_2 with three silanes to optimize the obscurant qualities of the powder. The LabRAM acoustic mixer helps in agitating the dry powder TiO_2 to expose more surface area for the silane to coat. The best mode was found with N-OTMS coated material giving a yield of 60% and gFOM of 1.91 m^2/cm^3, a 2x improvement over the base RCL-9 material. DPDMS, which we believed to have the highest potential given previous results, did

poorly in the packed format chamber launch, having a very low yield (18% vs. 60%). There are many variables that can affect the performance of the treated TiO_2 and we are currently exploring them by reconfiguring our LabRAM coating setup to allow for more complete control in temperatures and flow rates.

Figure 5.8: Geometry that mimics M106 geometry and gas (1L) volumes results in substantial degradation of gFOM.

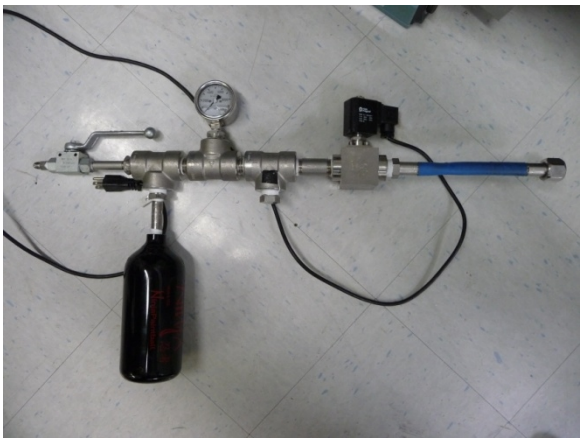

Figure 5.9: Optimized 10 mL, high volume launch format using 120L gas.

5.2.1.2 10 mL, 1 gram format

To further improve the gFOM, modifications were made to the launch mechanism and packed powder format to increase the yields and reduce agglomeration. Instead of a narrow cylinder with a thick column of powder that mimics the M106 geometry, a shorter and wider format was used (**Figure 5.7, center**). In this format, combined with more gas flow, the yields are greatly improved. Duplicates of each material were loaded into 10 mL devices, each with 1 gram, packed to a pressure of 500 psi, and launched with an optimized high pressure solenoid valve (**Figure 5.9**). Spectral extinction performance of the materials is shown in **Figure 5.10**. The **Table 5.6** summarizes the performance, showing averages of the two launches with a standard deviation. This modified launch configuration doubled the performance of the highest performing materials. The best mode for the surface modified material was found with the cyclic azasilane coatings, giving very high yields of 92.9%, MEC in the visible of 1.92 m^2/g, and a gFOM of 3.73 m^2/cm^3, a 50% improvement over the uncoated RCL-9. Comparisons with the CR-470 material currently used in the M106, when packed and dispersed in the same manner yields a very high gFOM of 4.6 m^2/cm^3. This finding is surprising, but may suggest that the CR-470 material may be a good candidate for further processing and surface coating to reduce agglomeration of particles and thus increase the MEC value. The cyclic azasilanes have the potential to be an even better surface, either applied over the alkoxy silane or after stripping the surface with acid and then applying.

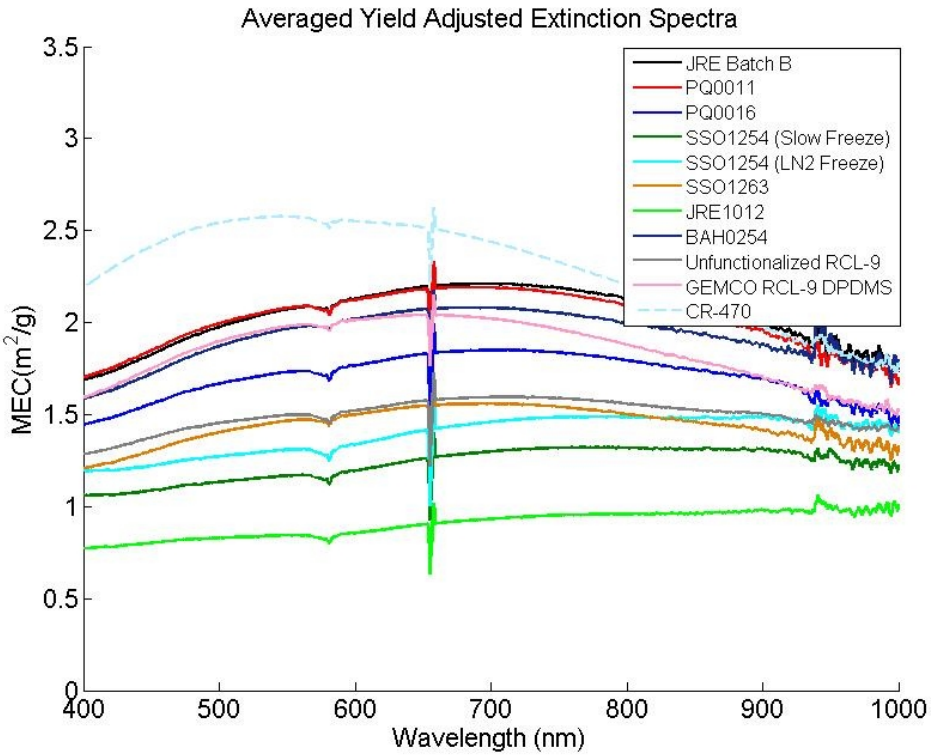

Figure 5.10 Spectral mass extinction performance of surface modified TiO_2 launched in a packed format.

Sample	Surface	Pressure (PSI)	Fill Fraction	Yield	MEC (0.4-0.7μm) avg	FOM avg	FOM stdev
TiO2 CR-470	alkoxy silane	500	46.1%	99.0%	2.49	4.60	0.71
TiO2 BAH0254	cyclic azasilane	500	51.1%	92.9%	1.92	3.73	0.37
TiO2 GEMCO RCL-9 DPDMS	DPDMS	500	49.5%	87.0%	1.92	3.45	0.08
TiO2 JRE Batch B	NOTMS	500	54.1%	80.7%	1.90	3.35	0.39
TiO2 PQ0011	NOTMS	500	48.5%	82.0%	2.03	3.35	0.33
TiO2 PQ0016	NOTMS	500	44.4%	80.8%	1.70	2.71	0.36
TiO2 Unfunctionalized RCL-9	none	500	45.8%	81.1%	1.48	2.49	0.33
TiO2 JRE Batch A	NOTMS	500	46.3%	71.5%	1.77	2.20	0.16
TiO2 SSO1263	mag stearate, stearic acid	500	47.2%	75.0%	1.44	2.19	0.08
TiO2 SSO1254 (LN2 Freeze)	TEOS	500	26.7%	73.8%	1.31	1.02	0.07
TiO2 JRE1012	NOTMS	500	33.0%	82.4%	0.84	0.94	0.00
TiO2 SSO1254 (Slow Freeze)	TEOS	500	23.4%	78.3%	1.17	0.87	0.12

Table 5.6 Summary of performance of surface modified TiO_2 launched in a packed format.

5.2.2 Comparison with HC smokes

HC smokes have an average MEC of ~3 m^2/g (**Figure 3.1**). Liquid fill fractions are equal to 1 and the density of HC is calculated to be 3.5 m^2/g based on 45% HC (ρ = 2.09 g/cm^3), 45% ZnO (ρ = 5.06 g/cm^3) and 10% Al (ρ = 2.7 g/cm^3). gFOM is calculated to be 10.5 m^2/cm^3, which is still larger than the 4 m^2/cm^3 achieved for the surface modified particulate obscurants tested at nanoComposix. However, the 4 m^2/cm^3 is more than six fold larger than the fielded M106 and is still only ~20% of the maximum theoretical value of what could be obtained if individual TiO_2 nanoparticles of the correct size are aerosolized. With further improvement to deagglomeration, gFOM values greater than HC can be achieved.

5.3 Field testing with center burster explosives

Six grenades, four M106 grenades filled with 223 grams of surface functionalized RCL-9 TiO_2 and two grenades with unmodified RCL-9 TiO_2 were prepared to determine the effect of surface coating and different explosive dissemination mixtures on performance in a full scale test. The two explosive mixtures used were potassium perchlorate and aluminum binary mixture, which is the explosive fill used in the current M106, and 2,4,6-trinitrophloroglucinol (TPG), an explosive formulation developed by Capco. The TPG burster is a pyrotechnic explosive that generates TiO_2 particles when detonated that not only disperse the obscurant fill material, but also increase the visible obscuration of the device. Testing was done at Capco, Inc., a research, development, and manufacturing company located in Grand Junction, CO. Each device was filled with TiO_2 and lightly compressed to a pressure of 30 psi. The devices were packed were assembled in two stages. The first stage loaded 100 grams and was compressed to 30 psi with a washer stopper to retain the particle fill after release of pressure from the ram. A second load (123 grams) was added on top and compressed with a second washer to the final pressure of 500 psi. A final fill fraction of ~30% was obtained for all devices tested (**Table 5.7**).

NCX ID	Material	Center burster	Mass of Fill (g)	Fill Fraction (%)
NCX162	RCL-9 +nOTMS	KAP	222.9	31.2%
NCX163	RCL-9 +nOTMS	TPG	222.2	29.3%
NCX164	RCL-9 +nOTMS	KAP	222.6	30.8%
NCX165	RCL-9 +nOTMS	TPG	222.6	30.5%
NCX166	RCL-9	KAP	223	30.0%
NCX167	RCL-9	TPG	223	30.0%

Table 5.7: Full size M106 devices packed with TiO_2 and explosively disseminated in an outdoor range at CAPCO.

Figure 5.11: High speed video from device NCX165. a) t = 0, b) t = 0.116s, c) t = 20 seconds.

The devices generated a thick cloud of white smoke that decreased the transmission to < 50% for up to 40 seconds (**Figure 5.11**) providing a dense screening smoke for >20 seconds in the test area. Due to the outdoor testing environment and an intermittent wind, there was variability in both the absolute magnitude of the transmission drop and the temporal characteristics of launch (**Figure 5.12**). The device fill that had the highest performance for the longest duration was a n-OTMS coated TiO_2. All coated materials regardless of the explosive burster used had a higher performance than the uncoated materials. However, it was difficult to make any quantitative conclusions due to the uncontrolled test environment. Chamber measurements of the coated materials at full scale in a

chamber similar to the one at ECBC (190 m^3) would provide more definite measurements of MEC and gFOM.

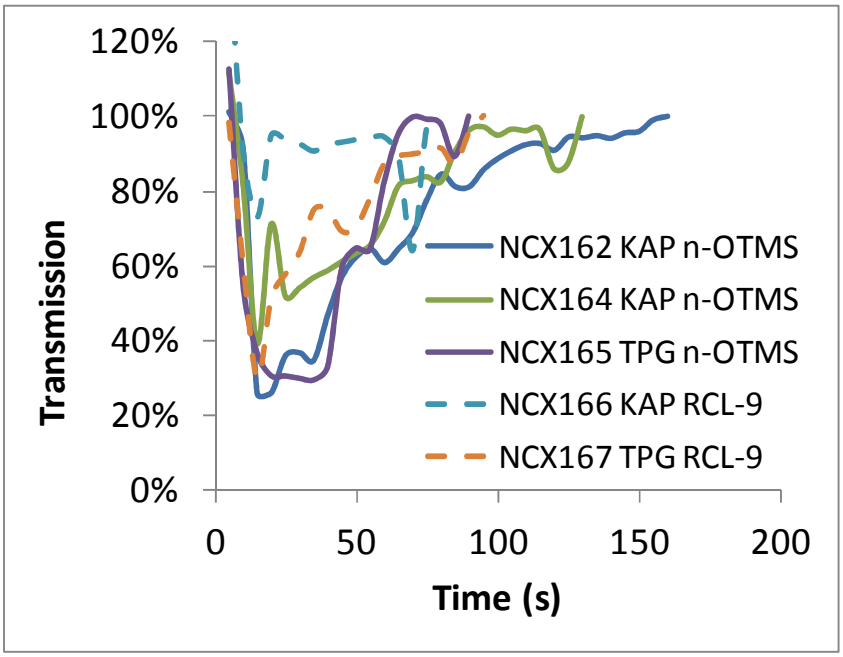

Figure 5.12: Results from full size M106 devices packed with TiO_2 and explosively disseminated in an outdoor range at CAPCO. Data captured with visible spectrophotometer.

5.4 Dissemination method development and results

Agglomeration of nanoparticles is a main factor in the reduction of the gFOM from theoretical limits. Chamber tests have shown that high shear SRI venturi pump nozzles are most effective at dissemination loose powders. However, fielded devices use a sub-optimal center burster configuration that typically has 15 – 30% yields. Here we investigated a pneumatic device using multiple nozzles of various configurations in order to increase the yields and deagglomeration.

5.4.1 Evaluate MAG device with smaller nozzle diameters with proxy material

5.4.1.1 Background:

The Multipurpose Aerosol Grenade (MAG) device is an ECBC designed metal re-usable cylinder that can eject powders using compressed gas through 6 converging/diverging nozzles in the top plate of the device (**Figure 5.13**). When a firing pin is pulled, a spring drives a sharp piston into the top of the CO2 cartridge, releasing the gas and ejecting the powder through the 6 nozzles. Powder is ejected over a 1-2 second period.

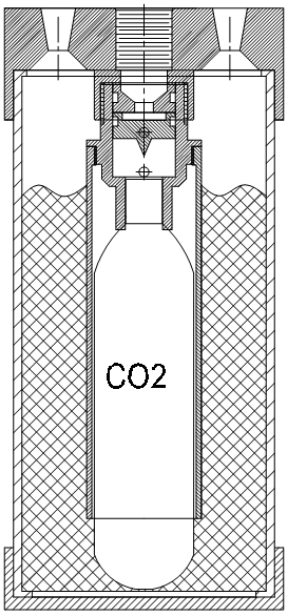

Figure 5.13: Sketch of MAG device. Upon firing, CO2 gas is released, flowing down the inner cylinder. The expanding gas ejects the powder through a series of nozzles in the top lid.

At nanoComposix, we fabricated a version of the MAG device that has removable plugs in place of the fixed outlet nozzles in the ECBC MAG design (**Figure 5.14**). This modification allows for customized nozzles to be easily interchanged within the device. One hypothesis is that decreasing the size of the nozzles and increasing the number of nozzles will create a higher degree of microturbulence leading to increased performance. To investigate the effect of nozzles on dissemination efficacy a series of nozzle configurations were tested. The original nozzle design used six nozzles with 5.1 mm diameter holes for a total area of 121.6 mm^2. New configurations were tested with combined nozzle areas of 70 mm^2, (60% of original area). As the size of the holes

was reduced, the number of holes used was increased to keep the cross sectional area constant (**Table 5.9**).

Figure 5.14: MAG device with modified lid using replaceable brass fitting nozzles.

Initial experiments were conducted using a center hole version of the MAG which allowed the use of air from a nitrogen tank connected to a solenoid instead of a CO_2 cartridge. One concept with the MAG device is that it could be engineered to pulse deliver air, effectively creating a more continuous delivery of obscurant material to more closely mimic burning grenades such as those based on HC smokes. Three pulses of air at 800 psi (CO_2 delivery pressure) with a 0.5 second duration were conducted for each test. Corn starch (100 g) was used as a proxy material for the initial tests.

Drill	Nozzle Diameter (mm)	Nozzle Area (mm^2)	Nozzle Quantity	Total Area (mm^2)	Notes
3/8	9.398	69.4	1	69.4	
4	5.334	22.3	3	67.0	
24	3.835	11.6	6	69.3	
48	1.930	2.9	24	70.2	
60	1.016	0.8	95	77.0	
-	5.080	20.3	6	121.6	Original MAG

Table 5.9: Test matrix. The diameter and number of the nozzles used were configured to conserve the total nozzle area.

The mass of the cylinder was measured before and after each burst to quantify the amount of material that was launched with each pulse and all ejections were captured on high speed video.

Each of the 6 different nozzle type was run in triplicate. 32 tests were conducted in total using both the corn starch surrogate and TiO2. The test results are shown below in **Table 5.10**:

ID	Duration (s)	Nozzle Qty	Nozzle Dia (in.)	Fill Mass (g)	Mass After Launch (g)	Mass launched (g)	Mass remaining (g)	Fraction Initial Launched	Fraction Remaining Launched
A				100	887.47		100.04		
JCH1301-A1	1	1	0.375	100	796.15	91.32	8.72	91.3%	91.3%
JCH1301-A2	1	1	0.375	100	789.4	6.75	1.97	6.7%	77.4%
JCH1301-A3	1	1	0.375	100	788.47	0.93	1.04	0.9%	47.2%
B				100	888.94		100.48		
JCH1301-B1	0.5	3	0.375	100	800.87	88.07	12.41	87.6%	87.6%
JCH1301-B2	0.5	3	0.375	100	791.81	9.06	3.35	9.0%	73.0%
JCH1301-B3	0.5	3	0.375	100	789.53	2.28	1.07	2.3%	68.1%
C				200	989.74		200.22		
JCH1301-C1	0.5	3	0.375	200	806.35	183.39	16.83	91.6%	91.6%
JCH1301-C2	0.5	3	0.375	200	793.19	13.16	3.67	6.6%	78.2%
JCH1301-C3	0.5	3	0.375	200	790.08	3.11	0.56	1.6%	84.7%
D				100	887.5		99.92		
JCH1301-D1	0.5	3	0.21	100	810.45	77.05	22.87	77.1%	77.1%
JCH1301-D2	0.5	3	0.21	100	796.09	14.36	8.51	14.4%	62.8%
JCH1301-D3	0.5	3	0.21	100	791.54	4.55	3.96	4.6%	53.5%
E				200	991.67		200.16		
JCH1301-E1	0.5	3	0.21	200	827.16	164.51	35.65	82.2%	82.2%
JCH1301-E2	0.5	3	0.21	200	798.65	28.51	7.14	14.2%	80.0%
JCH1301-E3	0.5	3	0.21	200	792.4	6.25	0.89	3.1%	87.5%
F				100	892.01		100		
JCH1301-F1	0.5	6	0.151	100	807.48	84.53	15.47	84.5%	84.5%
JCH1301-F2	0.5	6	0.151	100	795.11	12.37	3.1	12.4%	80.0%
JCH1301-F3	0.5	6	0.151	100	791.75	3.36	-0.26		108.4%
G				100	891.04		100.2		
JCH1301-G1	0.5	3	0.151	100	829	62.04	38.16	61.9%	61.9%
JCH1301-G2	0.5	3	0.151	100	799.34	29.66	8.5	29.6%	77.7%
JCH1301-G3	0.5	3	0.151	100	x	x	x	x	x
H				200	991.72		200		
JCH1301-H1	0.5	3	0.151	200	852.95	138.77	61.23	69.4%	69.4%
JCH1301-H2	0.5	3	0.151	200	809.2	43.75	17.48	21.9%	71.5%
JCH1301-H3	0.5	3	0.151	200	795.8	13.4	4.08	6.7%	76.7%
I				100	893.17		100.04		
JCH1301-I1	0.5	1	0.151	100	876.38	16.79	83.25	16.8%	16.8%
JCH1301-I2	0.5	1	0.151	100	853.35	23.03	60.22	23.0%	27.7%
JCH1301-I3	0.5	1	0.151	100	838.56	14.79	45.43	14.8%	24.6%
J				100	893.34		100		
JCH1301-J1	3	1	0.151	100	800.55	92.79	7.21	92.8%	92.8%

ID	Duration (s)	Nozzle Qty	Nozzle Dia (in.)	Fill Mass (g)	Mass After Launch (g)	Mass launched (g)	Mass remaining (g)	Fraction Initial Launched	Fraction Remaining Launched
K				100	889.7		100.08		
JCH1301-K1	0.5	24	0.076	100	805.24	84.46	15.62	84.4%	84.4%
JCH1301-K2	0.5	24	0.076	100	792.58	12.66	2.96	12.6%	81.0%
JCH1301-K3	0.5	24	0.076	100	789.91	2.67	0.29	2.7%	90.2%
L				100	891.66		100.28		
JCH1301-L1	0.5	95	0.04	100	804.77	86.89	13.39	86.6%	86.6%
JCH1301-L2	0.5	95	0.04	100	793.87	10.9	2.49	10.9%	81.4%
JCH1301-L3	0.5	95	0.04	100	791.03	2.84	-0.35	2.8%	114.1%
M				200	991.07		200.02		
JCH1301-M1	0.5	95	0.04	200	802.51	188.56	11.46	94.3%	94.3%
JCH1301-M2	0.5	95	0.04	200	792.37	10.14	1.32	5.1%	88.5%
JCH1301-M3	0.5	95	0.04	200	790.25	2.12	-0.8	1.1%	160.6%
N				100	892.35		100.14		
JCH1301-N1	0.5	3	0.21	100	824.03	68.32	31.82	68.2%	68.2%
JCH1301-N2	0.5	3	0.21	100	802.2	21.83	9.99	21.8%	68.6%
JCH1301-N3	0.5	3	0.21	100	795.44	6.76	3.23	6.8%	67.7%
O				100	895.64		100.22		
JCH1301-O1	4 x 0.5 sec pulses	3	0.21	100	793.34	102.3	-2.08	102.1%	102.1%
P				100	890.55		100.19		
JCH1301-P1	4 x 0.5 sec pulses	95	0.04	100	787.46	103.09	-2.9	102.9%	102.9%
Q	RCL-9 TiO2			200	989.39		200.12		
JCH1301-Q1	0.5	95	0.04	200	872.55	116.84	83.28	58.4%	58.4%
JCH1301-Q2	0.5	95	0.04	200	794.31	78.24	5.04	39.1%	93.9%
JCH1301-Q3	0.5	95	0.04	200	793.11	1.2	3.84	0.6%	23.8%

Table 5.10: Summary table of test configurations and results for MAG testing.

5.4.1.2 Nozzle geometry to optimally deagglomerate powder while maximizing total ejection rate

Multiple small nozzles were found to be more effective than a single large nozzle at deagglomerating particles. By conserving the surface area, no reduction in mass ejection was found even using nozzle diameters as small as 1.0 mm (Test M), see **Table 5.10**, **Figures 5.15-17**.

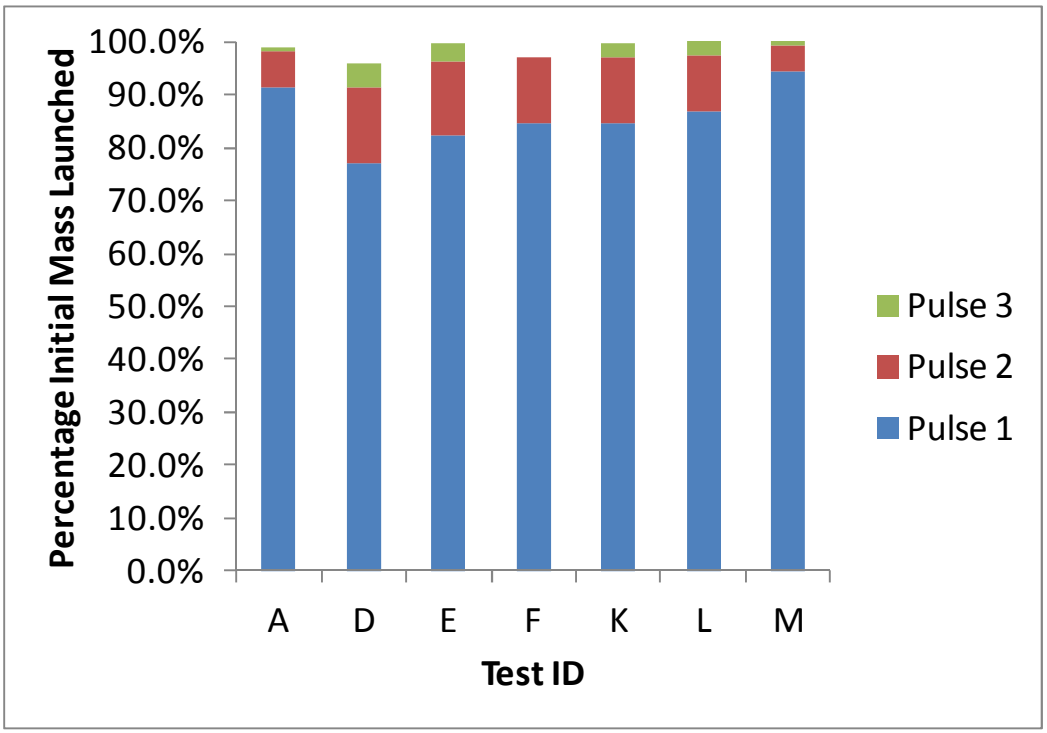

Figure 5.15: Summary of mass launched during each test with various nozzle diameters. Each pulse was 0.5 seconds of 800 psi N_2 gas.

Figure 5.16: Initial ejection of proxy material through 3 nozzles.

Figure 5.17: Initial ejection of proxy material through 95 nozzles.

5.4.1.3 Nozzle geometry to sequentially launch powder over time

A single nozzle with diameter 3.8 mm launched equal amounts (23 ±5.6 grams) during each 0.5 second pulse (Test I), **Figure 5.18**. This is a useful configuration when coupled to a pulsed gas source to provide a semi-continuous smoke device.

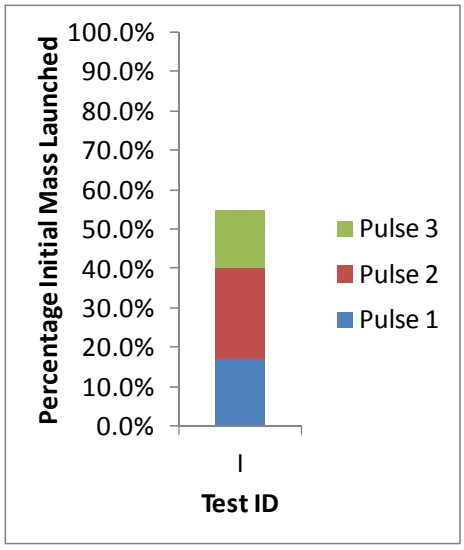

Figure 5.18: Equal mass amounts launched during sequential pulses using 1/3 the nozzle area of other tests.

5.4.1.4 Effect of fill mass on ejection rate (200 grams vs. 100 grams)

Four tests to investigate how the fill mass (and hence volume in the MAG) affects the percentage of mass ejected were performed using nozzles from 1.0 mm diameter to 9.5 mm diameter (**Table 5.11**). The tests compared launches of 200 grams to 100 grams using standard conditions of 0.5 second 800 psi N_2 gas.

Duration (s)	Nozzle Qty	Nozzle Dia (mm)	Additional mass launched (200 g vs 100 g)
0.5	3	9.5	3.9%
0.5	3	5.3	5.1%
0.5	3	3.8	7.5%
0.5	95	1.0	7.6%

Table 5.11: Effect of fill mass on ejection rate.

The percent of initial mass ejected during the initial 0.5 second pulse was 3.9% to 7.6% higher for 200 g mass loading vs. 100 gram, indicating that tests at the 100 grams scale are representative of full devices.

5.4.1.5 Validation with TiO_2

Table 5.12 shows a comparison of corn starch and RCL-9 TiO_2 launched using 95 nozzles of 0.8 mm diameter using 0.5 second pulses of 800 psi N_2 gas (**Figure 5.19**). In both cases > 98% of the initial 200 grams were launched after the first two pulses. 94% of the corn starch was launched in the first pulse, while 58% of the TiO_2 was launched after the first pulse (**Figure 5.20**).

ID	Duration (s)	Nozzle Qty	Nozzle Dia (in.)	Mass launched (g)	Mass remaining (g)	Fraction Inital Launched	Fraction Remaining Launched
M	Corn Starch				200.02		
JCH1301-M1	0.5	95	0.04	188.56	11.46	94.3%	94.3%
JCH1301-M2	0.5	95	0.04	10.14	1.32	5.1%	88.5%
JCH1301-M3	0.5	95	0.04	2.12	-0.8	1.1%	160.6%
Q	RCL-9 TiO2				200.12		
JCH1301-Q1	0.5	95	0.04	116.84	83.28	58.4%	58.4%
JCH1301-Q2	0.5	95	0.04	78.24	5.04	39.1%	93.9%
JCH1301-Q3	0.5	95	0.04	1.2	3.84	0.6%	23.8%

Table 5.12: Comparison of corn starch proxy material and TiO_2.

Figure 5.19: Corn starch 189 grams (of 200 g) launched during 0.5 second 800 psi N_2 pulse (Test M1).

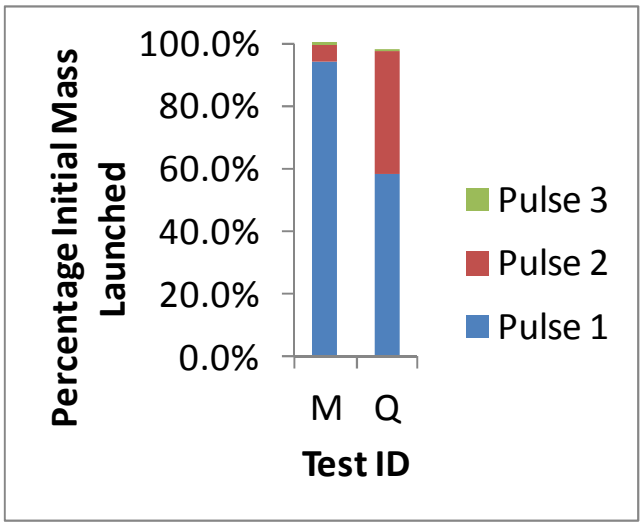

Figure 5.20: 98% of initial mass was launched during first two pulses for both corn starch and TiO_2.

5.4.2 Size characterization of TiO_2 particles launched by MAG device

Outdoor testing is useful to determine the mass ejection rates of powders from the MAG device as a function of air pressure and duration. However, the critical question that we were trying to address is whether a nozzle configuration can be identified that is more effective at deagglomerating the ejected powder. A 160 m^3 indoor testing chamber was used to evaluate the aerosolized particle size of different nozzle configurations. The MAG device was filled with 100 grams of TiO_2 (RCL-9) and launched at a 45 degree angle from vertical, diagonal across room. Two box fans spinning at medium speed were positioned near the launch platform. Aerosol size data was collected using an Aerosol Particle Sizer (APS) from TSI, Inc. through ¼" conductive tubing, 1 meter long, sampling through a side chamber port. Video of each launch was collected for 15 minutes, and then a large air volume HEPA filter was turned on to remove aerosolized particles from the chamber. After 30 minutes the air in the chamber was effectively purified.

For all tests the obscurant was well mixed 10 seconds after launch. Sample JCH1317A, the 95 nozzle launch configuration, launched 52.36 grams with a mass mean diameter of 3.20 µm and total

concentration of 1.82 mg/cm^3(**Table 5.13**). Sample JCH1317B, the 3 nozzle launch configuration, launched 44.85 grams with a mass mean diameter of 4.17 µm and total concentration of 2.74 mg/cm^3. Particle size distributions are shown in **Figure 5.21**. The total mass launched was similar for each configuration. JCH1317B produced a higher particle concentration than that of the JCH1317A, though the mean particle size was larger too 2.74 vs. 1.82 mg/cm^3. Visual frames are shown in **Figures 5.22-25** prior to launch (t = 0 seconds) and after the sample is well mixed (t = 10-15 seconds). Based on this data, nozzle diameter and number alone are not sufficient to dramatically change the performance of the M106 device. Different configurations that create additional turbulence (such as a converging nozzle or intersecting streams) may increase both aerosolized particle number and decrease average particle size.

Launch	Nozzles (#)	Nozz Dia. (in)	Mass TiO_2 (g)	Mass Launched (g)	Mass Mean Diameter (µm)	Total Concentration (mg/cm^3)
JCH1317A	95	0.040	100	52.36	3.20	1.82
JCH1317B	3	0.210	100	44.85	4.17	2.74

Table 5.13: Samples prepared and launched.

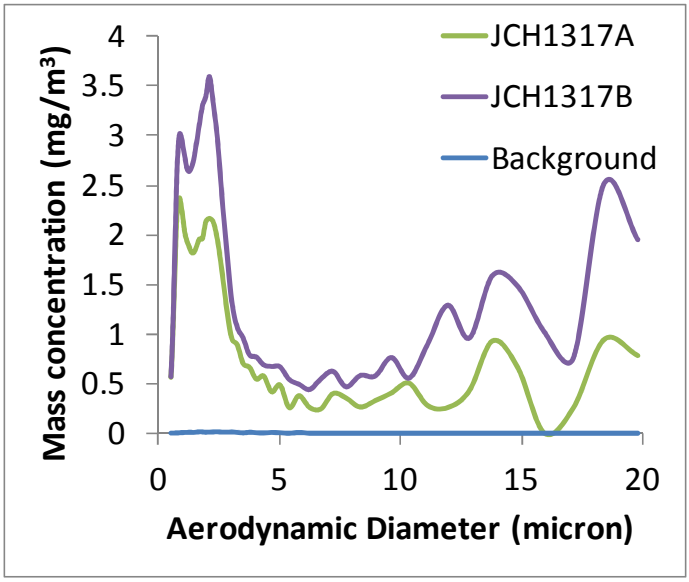

Figure 5.21: Aerodynamic particle size distribution for two TiO_2 samples, weighted by mass.

Figure 5.22: JCH1317A t=0 sec

Figure 5.23:JCH1317A t=15 sec

Figure 5.24: JCH1317B t=0s

Figure 5.25: JCH1317B t=10s

6 Conclusions and Implications for Future Research

Through a combined approach of surface modifications and dissemination development, nanoComposix was able to generate a low toxicity obscurant cloud with 6 times the performance of the currently fielded M106 device. Surface functionalization techniques were developed to functionalize TiO_2 in both a liquid suspension and as a dried powder. Both of these methods would be cost-effective at scale and were demonstrated to provide up to factors of 2 improvement off of an uncoated TiO_2 powder. High microturbulence generating launch formats demonstrated that large increases in gFOM can be obtained if a powder is disseminated with high energy and large shear forces. Combining the surface functionalization and the improved disseminations increase the gFOM from 0.6 m^2/cm^3 in the fielded M106 to over 4 m^2/cm^3 as measured in our aerosol chamber. Based on our calculation the obtained value is still only 20% of what can theoretically be achieved and continued improvement on fabrication, functionalization, drying, packing and disseminating nanoengineered obscurant powders has the potential to dramatically increase future performance of obscuration devices.

Further increases in obscuration performance can be obtained by additional modification to TiO_2 nanoparticles. Initial starting materials for all experiments performed during this contract were agglomerated – new methods to produce unagglomerated TiO_2 or to utilize ultra-high shear milling techniques (e.g. Kotobuki Ultra Apex Mill) to de-agglomerate TiO_2 powders will produce higher quality starting materials. While differences in performance of hydrophobic and hydrophilic surface coating were observed, there is a vast array of difference surface that may have superior anti-stiction properties including many of the surface coatings that are used as anti-caking agents and anti-sieze compounds. Chemical processing methods to functionalize TiO_2 with difference

surface coatings may dramatically improve performance. For materials that are in solution, novel drying techniques such as freeze drying or supercritical CO_2 drying have demonstrated improved powder dispersion performance. Dispersants that can be added and mixed with the TiO_2 before packing may also improve aerosolization. A large drop in performance is due to the center burster configuration of the M106 – different geometries or different explosive mixtures may more closely mimic the aerosolization performance that is obtained in our chamber. Given that the current M106 is only obtaining ~2.5% of the theoretical performance (0.6 m^2/cm^3 vs. 25 m^2/cm^3), further research on how to improve this safe and inexpensive obscurant material is justified.

This was achieved despite working with commercial powders that were agglomerated. Further gains could be had by using recently developed methods to mill particles in solution to primary size prior to surface medications, drying, processing, and packing. If the agglomeration and dispersion problems can be solved, there is the potential for devices with gFOM greater than that of HC (10.5 m^2/cm^3).

7 Literature Cited

Arkles, B., Pan, Y., Larson, G.L., Berry, D.H. Cyclic azasilanes: volatile coupling agents for nanotechnology, Silanes and Other Coupling Agents, 2004,Vol. 2, pp. 179-191. Ed. K.L. Mittal

ATSDR, Toxicological Profile for Hexachloroethane, A.f.T.S.a.D. Registry, Editor. 1997, U.S. Department of Health and Human Services, Public Health Service.

ATSDR, Toxicological Profile for Zinc, A.f.T.S.a.D. Registry, Editor. 2005, U.S. Department of Health and Human Services, Public Health Service: Atlanta, GA.

Brown, R. F., et al. The histopathology of rat lung following exposure to zinc oxide/hexachloroethane smoke or installation with zinc chloride followed by treatment with 70% oxygen. Environmental Health Perspectives 85 (1990): 81.

Cullumbine, H., The toxicity of screening smokes. J R Army Med Corps, 1957. 103(3): p. 119-

DeLacy 2011 Optical, Physical, and Chemical Properties of Surface Modified Titanium Dioxide Powders, ECBC-TR-835

DeVaull, G.E., W.E. Dunn, J.C. Liljegren, and A.J. Policastro, Analysis Methods and Results of Hexachloroethane Smoke Dispersion Experiments Conducted as Part of Atterbury-87 Field Studies., A. Argonne National Laboratory, Ill., Editor. 1989, U.S. Army Medical Research and Development Command, Fort Detrick, Frederick, Md.: Fort Detrick, Frederick, Md.

Donohue JM, G.L., Kirman C, Roberts WC, Zinc Chloride Health Advisory. 1992, Office of Water, U.S. Environmental Protection Agency, Washington, D.C., and the U.S. Army Medical Research and Development Command, Fort Detrick, Frederick, Md.

Hartman, D., Smoke and Obscurants Engineering Handbook, Volume II: Materials Characteristics, E.R.D.a.E. Center, Editor. 1995, US Army Chemical and Biological Defense Command: Orlando, FL. p. 68.

Hill, H.G., and K. Wasti, A Literature Review–Problem Definition Studies on Selected Toxic Chemicals. Occupational Health and Safety and Environmental Aspects of Zinc Chloride, Vol 5. 1978, Franklin Institute Research Laboratories: Philadelphia.

Hiroyoshi Yoden and Naoki Itoh, 2004, Effect of Small Size Beads on Dispersion of Nanometer-Sized Silica Particle by Wet Bead Mill Process, Journal of the Society of Powder Technology, Japan, vol. 41

Katz, S., Snelson, Alan, Farlow, Raleigh, Welker, Roger, Mainer, Stephen, Physical and Chemical Characterization of Fog Oil Smoke and Hexachloroethane Smoke. 1980.

Loh, C.H., et al., Case report: Hexachloroethane smoke inhalation: A rare cause of severe hepatic injuries. Environmental Health Perspectives, 2006. 114(5): p. 763-765.

NRC, Toxicity of Military Smokes and Obscurants, N.R. Council, Editor. 1997, National Academy Press.

Selden A., K.A., Bodin L. et al., Health effects of low level occupational exposure to hexachloroethane. Journal of Occupational Medicine and Toxicology 1994. 3(10): p. 73-79.

Zhu, M., Lerun, M.Z., Chen, W. How to prepare reproducible, homogeneous, and hydrolytically stable aminosilane-derived layers on silica. Langmuir 2012,28,416-423